Experimental and numerical studies of six small-scale continuous concrete slabs subjected to travelling fires

Experimental and numerical studies of six small-scale continuous concrete slabs subjected to travelling fires

Yong Wang [a*], Zhaoqing Ren [a], Zhaohui Huang [b,c], Wanyang Gao [a, d], Bo Zhong [e], Yixiang Bu [a], Yuner Huang [f], Yajun Zhang [a], Guanglin Yuan [a], Shuai Ma [a]

[a] *Jiangsu Key Laboratory of Environmental Impact and Structural Safety in Engineering, China University of Mining & Technology, Jiangsu, 221008, China;*

[b] *School of Civil Engineering, Xi'an University of Architecture and Technology, Xi'an 710055, China*

[c] *Vulcan Solutions Limited, Sheffield, S32 1DA, UK;*

[d] *School of Naval Architecture, Ocean and Civil Engineering, Shanghai Jiao Tong University, Shanghai 200240, China;*

[e] *Sichuan Fire Research Institute of MEM, Chengdu, Sichuan 610036, China*

[f] *School of Engineering, University of Edinburgh, Edinburgh EH9 3FG, UK*

Abstract

This paper presents the experimental results of six small-scale continuous reinforced concrete slabs with three compartments subjected to various compartment fire scenarios. The study investigates the influence of several key factors, including concrete age, thickness (span-thickness ratio), applied loads, and fire scenarios, on the fire behaviour of the continuous slabs. A nonlinear finite element program, Vulcan, was used to predict the fire behaviour of three tested slabs where spalling did not appear. The results indicated that increasing the slab thickness is one of the most effective methods for enhancing the fire resistance performance of continuous slabs subjected to any fire scenario. As the span-thickness ratio increased, the applied load had an increasingly significant effect on the deflection trend and maximum deflection of each span in the continuous slab. The conventional temperature failure criteria should be modified to consider the detrimental effects of fire-spreading scenarios, particularly the effects of a time delay and the direction of fire spreading. The numerical results revealed that, for any fire scenario, larger thermal straining leads to a larger mid-span deflection in continuous slabs subjected to various travelling fires.

Keywords: continuous slab; compartment fire; fire spread; load; time delay; numerical analysis.

1. Introduction

In recent years, the tensile membrane action of reinforced concrete slabs subjected to fire has been investigated via experimental and numerical studies, with a particular focus on simply supported slabs with large deflections. For instance, Lim et al. [1], Bailey et al. [2], Dong and Zhu [3], and Wang et al. [4-5] conducted full-scale or small-scale fire tests on isolated reinforced concrete two-way slabs with different restraint conditions. In addition, researchers have conducted fire tests on one-way and two-way continuous slabs to investigate the effect of continuity on the fire behaviour of the slab. Chen [6], Gao et al. [7], Yuan et al. [8], and Hou et al. [9] investigated the fire response of continuous reinforced concrete slabs and continuous prestressed slabs and found that the fire scenario has a significant influence on the position of the plastic hinge (i.e., the failure mode) in the continuous slabs. Meanwhile, several researchers [10-12] conducted four full-scale fire tests on different floor panels in a steel-frame building and found that three kinds of cracking patterns appeared on the top surface of the floor owing to the boundary conditions. However, it should be noted that all of the tests aforementioned involved uniform fire scenarios. Thus, their results cannot be easily extended to the evaluation of slabs subjected to travelling fires.

In 2019, Wang et al. [13] investigated the influence of various factors on the deflection, cracking pattern, and failure mode of four three-span continuous slabs (4700 mm × 2160 mm × 100 mm) subjected to different compartment fires. The factors evaluated included the fire spread direction, delay time, total fire duration, reinforcement ratio, and reinforcement arrangement. To investigate the effect of the number and position of the heated spans on the structural responses of the slabs, Wang et al. [14] further conducted five fire tests on three-span two-way continuous slabs (4700 mm × 2160 mm × 80 mm) subjected to single (two and three) compartment fires. The results showed that, for any fire scenario, increasing the reinforcement ratio and using continuous reinforcement are effective methods to prevent larger and wider cracks, particularly near to the supports of the continuous slabs. Thus, the fire resistant performance of the continuous slab is enhanced, such as the integrity and insulation. In this case, the effect of fire scenario (uniform or traveling fire scenario), reinforcement ratio and the position of the heated spans (boundary condition) should be considered to establish the reasonable temperature and deflection failure criteria, since the above factors have considerable influences on the temperature field (preheating behaviour) and deflection

(upward or downward trend) of each span in the continuous slab. However, the span-to-thickness ratios of the tested continuous slabs [13-14] were about 14 and 18, respectively, and the tensile membrane action could not be effectively mobilized in the continuous slabs owing to smaller mid-span deflections. In fact, conventional span-to-thickness ratios range from 20 to 40 [15]. Therefore, the present study aims to further investigate the effect of applied loads, concrete age, and fire duration. To contribute to the experimental database for numerical analysis, six small-scale tests were carried out on continuous slabs with dimensions of 4700 mm × 2160 mm × 50 mm subjected to various travelling fires. As discussed in reference [2], small-scale tests lead to higher temperatures or lower gradients in the slabs, but these results allow for the numerical models or theoretical methods to be validated, particularly in the cooling stage.

In addition to fire tests, many researchers developed different numerical models to analyse the membrane action of reinforced concrete slabs in fire. Lim et al. [16] applied the SAFIR software to analyse the mid-span deflection and membrane action of two-way slabs in fire. Results show that 3D analysis of two-way slabs using EC2 model showed agreement with fire test results, although the transient strain was implicitly considered. To develop a general concrete constitutive model, Wang et al. [17] established a correction function for the moisture content and improved the concrete constitutive laws for predicting the temperature and deflection of simply supported concrete slabs. It is found that during the heating stage, the effect of explicit transient strain on the deflection of the slab is negligible due to smaller compressive stress distribution. Huang [18] investigated the effect of spalling on the structural performance of concrete slabs in a fire. The model developed by Huang can be used to identify the upper and lower safety boundaries of concrete slabs with different support conditions. Meanwhile, Khalaf and Huang [19] developed a numerical model for analysing the bond-slip between concrete and reinforcing steel bars under fire conditions. The results indicated that the amount of concrete cover significantly affects the bond strength, by providing confinement to the reinforcement. Based on a plastic-damage formulation, Gernay and Franssen [20-21] developed a new multiaxial constitutive model for concrete (ETC model) at elevated temperatures to analyse the fire behaviour of concrete columns. Results show that the proper evaluation of the stiffness of the column requires an explicit computation of the transient creep. Hawileh and Kodur [22] conducted a numerical analysis on the fire behaviour of RC slabs

subjected to uniform hydrocarbon fire exposure and found that the load level has a considerable effect on the fire resistance of the RC slabs. Note that, the conventional temperature failure criteria (reinforcement temperature and temperature of unexposed concrete surface) may not be conservative under uniform hydrocarbon fire scenarios, since the deflection criterion (l/20) governed the failure of the analysed slabs under uniform hydrocarbon fire scenario. Thus, the effectiveness of the conventional failure criteria should be further verified by the tested slabs under traveling fire scenarios. Hajiloo and Green [23] predicted the temperatures (unexposed anchor zones), deflections, and bar stresses in GFRP-RC slabs and steel RC slabs. The results of their study showed that the coefficients of thermal expansion (CTE) for the concrete and reinforcing bars are the most significant parameters for predicting the deflection of the slabs. Meanwhile, the material strain failure criteria (concrete: 0.0035; steel: 0.05) and concrete tension stiffening effect were considered to determine the fire resistance of the slabs. Jiang and Li [24] investigated the mechanism and influencing factors (e.g., load ratio, boundary condition, slab thickness, reinforcement layout, and aspect ratio) related to the occurrence and development of tensile membrane action in RC slabs in a fire and suggested the deflection failure criterion of span/20 to predict the fire resistance of the slabs. In addition, five failure modes of the concrete two-way slabs were proposed based on the boundary conditions, orthotropic reinforcement layout and aspect ratios. However, the failure modes of the concrete slabs under the traveling fire scenarios may be different from those of the slabs under uniform fire scenarios due to different mechanical mechanism or deflection trend [13]. Thus, the failure modes of the continuous concrete slabs should be studied further based on the traveling fire tests.

It should be noted that the aforementioned numerical analyses of concrete slabs were mainly based on uniform fire scenarios. In addition, most of the studies only considered the fire performance of the concrete slabs during the heating phase. In reality, a cooling phase always exists after the peak temperature is reached. A fire often grows from its ignition source and travels throughout the floor until it is either extinguished or contained by compartment walls [25]. Thus, Law et al. [26] applied a novel methodology for defining a family of possible heating regimes to a framed concrete structure, using the concept of travelling fires. The results revealed that travelling fires have a significant impact on the performance of a structure and that current design approaches (i.e., temperature, deflection, and steel strain failure criteria) may not be

sufficiently conservative, and travelling fires have a more severe impact on the performance of the structure than the parametric fires. Thus, for the modern performance-based design, there is a clear need to address the shortcoming of the traditional design methods and establish the reasonable failure criteria of the concrete slabs under the traveling fire. In fact, Ellobody and Bailey [27] investigated the effect of different horizontal travelling fire scenarios on the fire behaviour of post-tensioned concrete slabs. They found that horizontally travelling fire scenarios and the associated time delay considerably affected the time-deflection behaviour. In terms of the maximum deflection, the worst case could occur either under a uniform fire or a travelling fire. Meanwhile, changes in the heating/cooling scenarios between zones resulted in a cyclic deflection pattern. However, it is noted that the cyclic deflection pattern was not observed from the middle spans in some tested slabs [13], and thus the above conclusion should be further verified by the traveling fire tests of the conventional concrete slabs with larger span-thickness ratios. Jiang et al. [28] investigated the effect of travelling fires on the thermal response of a large composite structure. The results indicated that travelling fires that are smaller in size produce higher peak temperatures in the concrete slab, and the maximum thermal gradients in the concrete slab seem to be insensitive to the location and size of the travelling fire. It should be noted that the EC2 model was often used in the mentioned numerical analyses, particularly in the heating stage. However, during the cooling stage, the effectiveness of the EC2 model requires further validation by the experimental results of concrete slabs, particularly under travelling fire scenarios.

Therefore, the main objectives of this study are: (1) to conduct six small-scale experiments on concrete continuous slabs subjected to different travelling fires; (2) to investigate the effects of an applied load, the span-thickness ratio, time delay, and total fire duration on the temperature, deflection, cracking patterns, and failure modes of the continuous slabs; and (3) to conduct a numerical analysis of the continuous concrete slabs using the EC2 model to verify its effectiveness in the cooling stage.

2. Test programme

2.1 Test specimens

In this research, the RC floor (three spans) of the prototype structure with the dimension of 11750 mm × 5250 × 125 mm and the concrete cover (reinforcement ratio) of 20 mm

(0.25%) was used. Using the Buckingham's principle of similitude, the specimen dimensions such as span length and sizes of slabs were scaled down by about 0.4 from a prototype building structure. Hence, six continuous slabs, each with dimensions of 4700 mm × 2100 mm × 50 mm, were fabricated in the laboratory. The concrete mix proportion and aggregate dimension (5-12 mm) are shown in Table 1. After curing at ambient temperature (20 °C) for 28 d, the concrete compressive strength was 34 MPa, while the yield and tensile strengths of the reinforcing steel bars were 439 MPa and 521 MPa, respectively. The diameter and cover of the steel bars were 4 mm and 8 mm, respectively, and they were set at 100 mm spacings, as shown in Fig. 1(a).

Other details of the six slabs (slabs CS1 to CS6) are shown in Table 2. As previously discussed, the span-thickness ratios (each span) of the tested slabs in references [13] (slabs B1 to B4) and [14] (slabs S1 to S5) were 14 and 18, respectively.

2.2 Instrumentation

As shown in Fig. 1(b), the furnace was operated by six oil-fired burner nozzles located in the south furnace wall, and each nozzle was controlled independently. The three smoke vents were located in the bottom furnace wall. As shown in Fig. 1(c), in each compartment, three Type K thermocouples (e.g. Points A-F-1 to A-F-3) were placed on the north furnace wall to measure the furnace gas temperature. The average of the gas temperature of each compartment was calculated from those values of three gas temperatures (e.g. Points A-F-1 to A-F-3).

Six Type K thermocouple trees were used to measure the slab temperatures within each compartment (Trees TA1 to TA6, TB1 to TB6, and TC1 to TC6), as shown in Fig. 1(d). For each thermocouple tree, the spacing between two thermocouples (e.g., Points 1 and 2) was 10 mm, and the top and bottom steel temperatures were measured using four thermocouples (i.e., Points R-1 to R-4), as shown in Fig. 1(e). As shown in Fig. 1(f), seven transducers were used to measure the vertical (Points VA, VB, and VC) and horizontal (Points H1, H2, H3, and H4) displacements of the tested slabs, respectively.

The uniform applied load (iron bricks) of each tested slab is shown in Table 2. The ultimate load carrying capacity (14 kPa) was predicted using yield line theory, and the corresponding load ratios were 0.16 (Slabs CS1 and CS2) and 0.30 (Slabs CS3 to CS6), respectively. In order to represent the behaviour of the slab under realistic support conditions in a typical building [1, 4, 5, 29], the four corners of each slab were

196 restrained using reaction beams, as shown in Figs. 2(a)-(c).

197 *2.3 Fire scenarios*

198 In the present study, six slabs were tested under different travelling or compartment
199 fires (i.e., fire scenarios). As shown in Table 2, to compare with the observation in
200 companion papers [13-14], the ISO834 fire and horizontal fire spread delay (45 min
201 and 90 min) were determined based on references [27, 30]. As discussed in Ref. [13],
202 the fire compartment wall is often used to avoid the rapid fire spreading within a
203 building, and its fire resistance time ranged from 15 min to 180 min. For instance, two
204 time delays (30 min and 60 min) were adopted to represent the fire spreading from one
205 span to another span. In this paper, the time delay 90 min was adopted to compare with
206 the results in Refs. [13-14]. The heating and cooling phases were controlled using
207 nozzles and cooling fans, and each test was stopped after 400 min (Table 2). The fire
208 scenario used for each slab is described below. The fire exposure times of the three
209 compartments in each fire scenario are listed in Table 2. The details of the different fire
210 scenarios are as follows:

211 (1) For slabs CS1 and CS2, only compartments A and B, respectively, were exposed to
212 fire for 180 min, and the other compartments were not heated. For slab CS6, each
213 compartment was heated for 90 min.

214 (2) For slab CS3, the three compartments were exposed to fire in a sequential order,
215 i.e., compartments A (0–90 min), B (90–180 min), and C (180–270 min). That is, only
216 one compartment was subjected to fire at a given time, with a time delay of 90 min.
217 Similarly, for slab CS5 with the same fire sequence and heating duration (90 min), the
218 time delay was 45 min.

219 (3) For slab CS4, compartment B was exposed to fire for the first 90 min, followed by
220 compartments A and C subjected to fire simultaneously for another 90 min.

221 **3. Experimental results**

222 *3.1 Furnace temperatures*

223 The average furnace temperature-time curves for the six slabs are shown in Figs. 3(a)–
224 (f). For instance, the ISO834 standard fire curve was used in the first heated span of
225 slab CS3, other spans were heated following the similar fire curve to conduct the
226 comparison. The maximum furnace temperature for each compartment is shown in

Table 3. It should be noted that the furnace temperatures in compartment CS6-C fluctuated with time owing to nozzle malfunction.

The furnace temperature of one compartment was observed to be dependent primarily on the ignition of the nozzles and the fire duration. At shut-off, the maximum furnace temperature of the heated spans ranged from 830 °C to 1137 °C. As expected, the shorter heating duration of slabs CS3 to CS6 (90 min) resulted in maximum furnace temperatures that were slightly lower than those of the previous tests [13-14]. For instance, the maximum furnace temperatures in slabs B1 to B4 [13] ranged from 1016 °C to 1299 °C, and those in slabs S1 to S5 [14] ranged from 1003 °C to 1147 °C, as shown in Table 3.

The furnace temperatures in the unheated compartments increased gradually up to the shut-off time (< 200 °C) and then remained constant during the cooling stages, as seen in compartments CS1-B-F and CS2-C-F (Fig. 3(a)).

3.2 Concrete and steel temperatures

Figs. 4(a)–(f) show the concrete temperatures of the six tested slabs, and the maximum concrete and steel temperatures are shown in Table 3. It should be noted that the data for compartment CS4-B were not measured owing to a malfunction of the thermocouples. In addition, the average bottom and top steel temperatures in each span are shown in Figs. 5(a)–(f).

The measured results indicate that there is no temperature plateau near the top surface of the slabs created for this study; this observation is different from those of the full-scale tested slabs in references [13-14]. As discussed above, the aggregate's dimensions (5-12 mm) were not reduced in size according to the reduction of the slab dimensions. In this case, the larger aggregates tend to increase the heat permeability and lead to the formation of concrete micro-crack [31]. Note that, concrete permeability is one of the most important characteristics controlling moisture transport. Meanwhile, micro-cracks tend to initiate in the high stress region and propagate along the weakest area to release stresses. Thus, no temperature plateau and large cracks appeared on the top surface of the tested slabs, respectively.

In fact, as will be discussed in Section 3.4, some steam was observed during the heating stage. Meanwhile, the average temperature (465 °C) after 90 min of heating was smaller than the temperatures measured (576 °C and 765 °C) in references [13-14] due to the

smaller slab thickness. Thus, for any fire scenario, the slab thickness has a considerable effect on the temperature gradient of the slab. Therefore, it can be concluded that increasing the thickness of a slab is an effective method for avoiding insulation failure in concrete slabs subjected to any fire scenario.

It was also observed that a time delay had a greater effect on the bottom steel temperature than on the concrete temperature of the later heated spans, particularly the maximum temperature during the heating stage. For slabs subjected to the same fire exposure duration, a longer time delay had no significant effect on the peak temperatures of the reinforcement compared with uniform fire scenarios. In slab CS3 and CS5, for instance, the maximum temperatures of bottom reinforcement in spans A, B, and C were 644 °C, 654 °C, and 721 °C, and 626 °C, 642 °C, and 673 °C, respectively, and the average values were 673 °C and 647 °C, respectively. However, the maximum temperature of bottom reinforcement in slab CS6 was 634 °C. In this case, for the travelling fire scenario, the later heated spans failed earlier than the first heated span. Thus, travelling fire scenarios, which include parameters such as the fire spread direction and time delay, should be considered to establish accurate temperature failure criteria for concrete slabs. This behaviour should also be considered in the post-fire damage assessment and repair of the later heated spans, owing to the lower residual material strength.

During the cooling stage, the concrete temperatures near the top surface of most of the slabs continued to rise, and the average duration of the rise (from the shut-off time) was about 21 min. However, the durations of the temperature rise in the tested slabs in references [13] and [14] were 84 min (100 mm) and 49 min (80 mm), respectively. Clearly, the increased thickness of those slabs resulted in a longer duration. In addition, for the slab with serious spalling, no temperature increase in the top surface appeared during the cooling stage, as observed in slabs CS1-A and CS2-B. This implies that, in the numerical model, the effect of spalling should also be considered to accurately predict the temperature of the slab during the cooling phase. Thus, this behaviour should also be considered in the failure criterion, post-fire performance assessment, and numerical (i.e., theoretical) analysis.

3.3 Deflection behaviour

The measured deflections were plotted against time and the furnace temperature, as

shown in Figs. 6(a)–(f) and Figs. 7(a)–(f), respectively. For the vertical deflections, the negative displacement is downward, and the positive displacement is upwards. For the horizontal deflections, the positive displacement is outward, and the negative displacement is inward.

3.3.1 Vertical displacements

- *Vertical displacement-time curves*

(1) Slabs CS1 and CS2

As previously mentioned, the load applied to slabs CS1 and CS2 was 1.0 kPa. Different from the downward deflections of all edge spans in references [13] and [14], the edge span of CS1-A first deflected downwards between 0 and 10 min, and then deflected upwards until 180 min. Its maximum mid-span deflection was 15 mm, indicating that the curvature of span CS1-A changed from sagging to hogging. It should be noted that such behaviour was not observed in the simply supported slabs or restrained slabs [1-6]. In other words, the applied load (1.0 kPa) was not sufficient to maintain a sagging curvature in the slab. This deflection behaviour led to cracks on the top surface and spalling on the bottom surface. As the applied load increased, the edge span of slabs CS3 to CS6 deflected downward during the heating stage, as will be discussed later. Ultimately, the applied load had a greater effect on the deflection trend in the thinner slab than on that in the thicker slab.

Similar to the observations in references [13-14], slab CS2-B deflected upward during the heating stage owing to the negative moment (i.e., boundary restraint) and displayed a maximum mid-span deflection of 21.9 mm. The middle span deflected upward, as its thermal expansion was restrained by the unheated spans. The upward deflection led to compressive stress on the bottom surface of the middle span, and, as a result, serious spalling occurred. It should also be noted that the upward deflection of span B decreased with an increase in the applied load (3.0 kPa), as seen in slabs CS3 to CS6. Thus, in terms of the maximum deflection, the effect of the applied load should be considered to determine the worst fire scenario for the middle span.

This observation is different from the results (i.e., downward deflections) of the isolated slabs [4-5], indicating that the interaction between the boundary restraint and applied load should be considered to establish reasonable deflection failure criterion for the floor, particularly for slabs with a larger span-thickness ratio.

(2) Slabs CS3 to CS6

The mid-span deflections for slabs CS3 to CS6 are shown in Figs. 6(c)–(f). The load applied to each slab was 3.0 kPa. Clearly, the deflection trend of the middle span in the continuous slabs was considerably dependent on the travelling fire scenario.

On one hand, the mid-span deflection of each edge span gradually increased with time, and the maximum mid-span deflection occurred at the shut-off time of heating. Meanwhile, the cyclic deflection pattern appeared in the edge span with the change in heating/cooling scenarios, which also occurred in references [13, 14, 27]. As shown in Table 3, the maximum mid-span deflection of the edge spans in slabs CS3 to CS6 at the corresponding shut-off time were −29.2 mm (span CS3-A), −32.3 mm (span CS3-C), −27.6 mm (span CS4-A), −27.2 mm (span CS4-C), −30.9 mm (span CS5-A), −28.0 mm (span CS5-C), −20.3 mm (span CS6-A), and −22.7 mm (span CS6-C), and the average mid-span deflection was −27.3 mm. It can be seen that the travelling fire spread direction and time delay had no significant effect on the maximum deflection of the edge spans, and the deflections mainly depended on the fire duration, furnace temperature, and applied load. In terms of the deflection failure criterion (l/50: 29 mm), the average fire resistance duration of the edge spans was about 90 min. However, it should be noted that most of the edge spans in references [13-14] did not fail, and their fire resistance durations were longer than 180 min. Thus, increasing the slab thickness may be the most effective method of enhancing the fire resistance of edge spans subjected to any fire scenario. In terms of the maximum deflection, it is easy to determine the worst fire scenario for the edge span in the structure, and the effect of the fire spread sequence or time delay can be neglected.

In contrast to the edge spans, the mid-span deflection of the middle spans was mainly dependent on the fire scenario (i.e., the fire spread order and time delay) and span-thickness ratio of the continuous slab. The maximum deflections of the middle spans for 15 fire tests are presented in Table 3. These deflections were smaller than those of the edge spans. On one hand, changes in the heating/cooling scenarios did not result in cyclic deflection patterns in the middle spans, which is different from the observations in reference [27]. For instance, different mid-span deflection trends in spans CS3-B (CS5-B), CS4-B and CS6-B were observed during the heating stage. On the other hand, different span-thickness ratios resulted in different deflection behaviours in the middle spans under similar travelling fire scenarios. For instance, span CS3-B (CS5-B)

deflected slightly upward until 90 (45) min, and then its downward deflection rapidly increased up to −23.9 (−10.9) mm at 180 (135) min. After the shut-off time, the deflection gradually recovered until the end of the test. However, span B3-B, which was subjected to a similar fire scenario (span-thickness ratio: 14) [13], deflected downward after ignition and then upward until 300 min. Thus, apart from the fire scenario, the span-thickness ratio was shown to have a significant effect on the deflection trend of the middle span in one continuous slab. Thus, it can be concluded that, for one span with higher boundary restraints, different travelling fire or uniform fire scenarios should be analysed to identify the worst fire case in terms of the maximum deflection. In other words, a higher furnace temperature or longer fire duration may not necessarily result in a larger deflection in the middle span. It also implies that the middle span tends to have experience integrity or insulation failure instead of deflection failure. In this case, owing to the complex deflection behaviour of the middle span, the designer could consider various influential factors (e.g., the time delay, fire spread order, applied load, and span-thickness ratio) to identify reasonable failure criteria and the worst case fire scenario.

As shown in Figs. 6(a)–(f), the deflection of each heated span rapidly recovered early in the cooling stage, and then remained constant later in the cooling stage. The final residual deflection of each span is shown in Table 3. Clearly, the residual mid-span deflection of the heated edge span was relatively larger than that of the heated middle span; this finding is similar to the results of references [13-14]. This comparison indicates that, apart from the heating phase, the boundary conditions have considerable effect on the residual deflection recovery of the continuous slab during the cooling phase. In this case, the collapse risk of the edge span may be larger than that of the middle span during the cooling phase owing to the larger residual deflection.

- Deflection-average furnace temperature curves

Figs. 7(a)–(f) show the mid-span deflection-average furnace temperature curves for slabs CS1 to CS6. On one hand, similar to the observations in references [13-14], the mid-span deflection of one edge span can be divided into two stages, and the turning point was at approximately 600 °C. Spans A and C were subjected to different fire scenarios, and their deflection trends with the furnace temperature were similar. Thus, for any travelling fire scenario, the furnace temperature can be used to evaluate the deflection stage of the edge span, particularly in the heating stage. On the other hand,

the deflection trend of the middle span was relatively complex, further indicating that the furnace temperature cannot be used by itself to determine the deflection stage. Ultimately, for a span with lower boundary restraints, there may be a single worst fire scenario; however, for a span with higher boundary restraints, there may not be a single worst fire scenario, owing to the interactions between several factors, as well as different failure mechanisms.

3.3.2 Horizontal displacements

Figs. 8(a)–(f) show the measured horizontal displacements for the six concrete slabs. The maximum horizontal displacements of the six slabs were 5.2 mm, 3.6 mm, 4.5 mm, 6.9 mm, 3.6 mm, and 9.5 mm, respectively, with an average value of 5.6 mm. Clearly, the horizontal displacements of the slabs created and tested in this study were relatively smaller than those (10.3 mm and 6.5 mm) in references [13-14], as a result of the shorter fire duration. Thus, compared with the furnace temperature and fire duration, the span-thickness ratio and applied load have no significant effect on the horizontal displacement of continuous slabs.

3.4. Cracking patterns and spalling

(1) Slabs CS1 and CS2

After 5 min, slab CS1 experienced serious spalling accompanied by a loud sound. Then, slight spalling was heard until 37 min. At 20 min, cracks appeared on the corners of the slab and the mid-span region of the top surface. It should be noted that some steam was observed on the top surface between 45 min and 50 min. The cracking patterns and spalling are shown in Figs. 9(a)–(d). Clearly, the short corner cracks mainly appeared on heated span A owing to its upward deflection, and fewer cracks appeared near its adjacent internal support. On the bottom surface, there were fewer short edge cracks around the heated region, with a maximum spalling depth (area) of 45 mm (0.98 m^2). In addition, the cracking pattern in span CS1-A was different than that of Span S1-A [14] as a result of a different deflection trend. It can be seen that the crack distribution and spalling may be used to evaluate the deflection trend of the span during a fire.

Beginning at 10 min, spalling occurred in slab CS2, until 47 min. It should be noted that at 34 min, sounds of serious spalling were heard and the sudden vibration of the slab was observed. In this case, less steam appeared on the top surface during the test. As shown in Figs. 10(a)–(d), owing to the upward deflection, many short-span cracks

appeared on the top surface of span CS2-B. The maximum spalling depth (area) was 42 mm (1.15 m^2), which was attributed to the lower concrete age. It should be noted that serious spalling occurred in span S2-B [14] (concrete age: 198 days). However, spalling did not occur in slabs B1-B to B4-B owing to older concrete age (about 724 days) [13]. A comparison indicated that the concrete age has a considerable effect on the extent of concrete spalling and should be considered while identifying the worst fire case.

(2) Slabs CS3 and CS4

For slab CS3, cracks and steam appeared in the middle region at about 25 min. At 67 min, the amount of steam on the top surface decreased. For span CS3-B, steam appeared at 109 min and gradually increased until 117 min. It should be noted that loud spalling occurred at 123 min, and no steam appeared at 149 min. For span CS3-C, steam appeared between 200 min and 236 min, and no spalling occurred during the test.

Figs. 11(a)–(d) show the symmetrical cracks on the top surface of slab CS3 and many short-span (south-north) cracks concentrated at the internal supports and in span CS3-B. Different from the many short-span cracks (upward deflection) in span B3-B [13], circular cracks appeared in span CS3-B owing to the downward deflection. There were fewer cracks (i.e., larger crack spacing) in span CS3-B because of its lower reinforcement ratio.

In slab CS4, cracks first appeared near two of the internal supports in span CS4-B, and steam appeared between 23 min and 66 min. Spalling occurred between 26 min and 44 min, and loud spalling was heard at 36 min. For span CS4-A, the spalling on the bottom surface appeared between 106 min and 130 min, and steam appeared between 110 min and 140 min. The results of the tests on the slabs for this study showed that steam appeared at about 20 min (from ignition), with a duration of about 40 min. It should be noted that for slabs B1 to B4 [13] (slabs S1 to S5 [14]), steam appeared at about 30 min (30), and continued over a duration of 90 min (30). This comparison indicates that the thickness has no significant effect on the initial evaporation time, but does have a considerable effect on the evaporation duration (or insulation failure).

As shown in Figs. 12(a)–(d), symmetrical cracks appeared on the top surface of slab CS4, with arc cracks at the two edge spans. It should be noted that no arc cracks were observed on the top surface of any edge span in references [13-14]. Thus, the span-

thickness ratio had a considerable effect on the appearance of edge arc cracks. In addition, spalling occurred on the bottom surface of span CS4-B (spalling area: 0.53 m^2; maximum depth: 36 mm), and slight spalling occurred on span CS4-A. Compared to slabs CS1 and CS2, the spalling in slab CS4 was relatively slight owing to its older concrete age (196 days).

(3) Slabs CS5 and CS6

During two of the fire tests, no steam (spalling) was observed as a result of higher concrete age of the slab (Table 2). The concrete ages of slabs B1 to B4 [13] (no spalling) ranged from 701 days to 749 days, and those of slabs S1 to S5 [14] (slight spalling) ranged from 189 days to 236 days. Therefore, it can be concluded that, for any fire scenario, serious spalling does not occur in slabs with a concrete age greater than 2 years, particularly in slabs with larger span-thickness ratios. However, for continuous slabs with a concrete age less than 1 year, spalling should be considered in the fire resistant design, particularly for the middle span.

Figures 13(a)–(d) and 14(a)–(d) show the symmetrical cracking pattern on the top and bottom surfaces of slabs CS5 and CS6, respectively, including the arc or inclined cracks (top surface) and short-span bottom surface cracks (internal supports). It can clearly be seen that the internal supports became the weakest region as a result of the increasing span-thickness ratio, and integrity failure occurred owing to the short-span top and bottom cracks.

4. Discussion

The authors conducted fire tests on 15 three-span reinforced concrete continuous slabs under various combinations of compartment fire scenarios [13-14]. The test variables included the fire spread sequence, fire duration, time delay, number of heated spans, reinforcement ratio, thickness, applied load, reinforcement cover, reinforcement spacing, and reinforcing bar diameter. Based on the aforementioned information, the following observations were made:

(1) Concrete and reinforcement temperatures

According to conventional concrete and reinforcement temperature failure criteria [14, 26, 32-33], the fire resistance of each heated span is shown in Table 4. Accordingly, the failure of one span is said to occur when: 1) the average temperature on the unexposed

surface of the span exceeds 140℃ or temperature at any one point exceeds 180℃ above initial temperature. 2) The temperature of the reinforcement near to the bottom surface of one span exceeds 593℃. For one span, the fire resistance was calculated from its ignition (i.e., direct heating). Clearly, the above failure criteria can be easily used to compare the impact of different traveling fires on the slabs, although this is a fairly arbitrary measure of failure [26].

For instance, the average fire resistance (concrete temperature failure criterion) of the first heated spans (spans CS3-A, CS5-A, CS6-A, CS6-B, and CS6-C) was 61.44 min, with an average fire resistance (steel temperature) of 74.7 min (spans CS3-A, CS5-A, and CS6-A). However, the average fire resistance of the last heated spans (spans CS3-C, CS4-A, CS4-C, and CS5-C) was 39.6 min (concrete temperature) and 69.1 min (steel temperature), respectively. The time delay led to reduced fire resistance in the later heated spans, with decreased ratios of 35.5% and 7.50%, respectively. As discussed in reference [13] and according to the temperature failure criteria for the concrete vs. reinforcement, the average fire resistance of the first heated span of slabs B1, B3, and B4 was 155.6 min vs. 157.1 min, and the fire resistance of the last heated span was 121.9 min vs. 116.3 min, with decreased ratios of 21.7% vs. 26.6%, respectively. A comparison of these values reveals that the fire spread or time delay has a considerable effect on the fire resistance of the later heated spans with smaller thickness. Thus, in the travelling fire scenario, earlier failure (i.e., lower fire resistance) easily occurs in the later heated spans of the continuous slab as a result of preheating. Consequently, the detrimental effects of the travelling fire scenario on the fire resistance of the floor should be considered in the design. Otherwise, the fire resistance of the later heated spans will be overestimated, particularly for thinner slabs.

During the cooling stage, the top surface temperatures of slabs CS1 to CS6, slabs S1 to S5 [14], and slabs B1 to B4 [13] reached the corresponding maximum values after about 21 min, 49 min, and 84 min, respectively. Thus, for travelling fire scenarios, the time required to reach the peak temperature can not only depend on the distance relative to the origin of the fire [26-27], but also on the thickness of the slab. This observation indicates that, during the cooling stage, thicker slabs have increased insulation and integrity failure risk, as it takes more time to reach the peak temperature.

(2) Deflection behaviour

In accordance with the deflection failure criterion (l/50), the fire resistance of each heated span is given in Table 4. On one hand, in all of the fire scenarios [13-14], the heated middle span did not fail, as a result of higher boundary restraints. On the other hand, with the exception of span CS1-A, the fire resistance of most of the edge spans was about 90 min, being smaller than those in references [13-14], as indicated in Table 4. Thus, it can be concluded that increasing the slab thickness is one of the most effective methods of enhancing the fire-resistance performance of continuous slabs. The effects of the boundary restraints and applied loads should be considered in the fire resistance determination.

The worst fire scenario of each span in a continuous slab is discussed regarding the deflection behaviour. On one hand, during the heating stage, the deflection trend of the edge span was not significantly affected by the fire spread, time delay, span-thickness ratio, or applied load. With the exception of span CS1-A, which had a smaller applied load, the edge spans of the other slabs deflected downward. It was observed that, for one continuous slab, the maximum deflections in the edge spans were mainly dependent on the furnace temperature and fire duration (i.e., the temperature gradient and material properties). In this case, in terms of the deflection, the worst fire scenario for the edge span could be easily determined (i.e., higher furnace temperature, longer fire duration, and larger applied load). On the other hand, the deflection in the middle span was dependent on the interaction between many factors, including the fire scenarios, location and number of heated spans, span-thickness ratio, applied loads, spalling, etc. In this case, for the middle span, a series of uniform or travelling fire scenarios should be considered to identify the worst fire scenario.

During the cooling phase for any of the fire scenarios, the entire deflection trend of the edge and middle spans gradually recovered with time. Compared with the edge spans, the fire spread scenario had a considerably greater impact on the residual deflection trend and recovery ratio of the middle span. For instance, different deflection recovery trends were observed in spans CS3-B and CS4-B. Thus, the failure mechanisms (i.e., mode) were different (i.e., flexural behaviour and arc action). Consequently, the effect of the travelling fire scenario on the residual deflection behaviour of the middle span should be considered in the post-fire assessment or repair, as different fire cases may lead to a different failure mechanism or cracking pattern during the fire [34].

(3) Failure mode

The cracking pattern, spalling, and failure mode of 15 tested slabs were compared. The top surface cracks of the tested slabs were mainly concentrated on the heated spans and their adjacent internal supports. As the span-thickness ratio increased, the cracks through the thickness appeared near the internal supports. As the three spans of one continuous slab were heated sequentially or simultaneously, the final crack pattern on the top surface of a slab with any span-thickness ratio or any fire spread scenario became symmetrical. Thus, for uniform or travelling fire scenarios, the boundary conditions should be considered to accurately determine the cracking pattern of each span in the continuous slab. However, according to the cracking pattern or failure characterises, the overall deflection trend (upward or downward) and mechanical mechanism (arch action or tensile membrane action) could be deduced during the fire (such as in slabs CS3 and CS4) and could be used to assess the residual performance or determine reasonable repair methods.

Compared with the fire scenario and boundary conditions, the concrete age may actually be the most important factor that influences the occurrence of spalling. Essentially, if the concrete age of a slab subjected to any fire scenario is greater than two years, the spalling in any span can be neglected. However, if the concrete age is less than half a year, the spalling in each span should be considered in the fire-resistance design, particularly in the middle span. When the concrete age ranges from half a year to two years, the spalling in the middle span should be conservatively considered in the fire-resistance design.

5. Numerical analysis

The Vulcan program [18] was used to predict the temperature and deflection for three tested slabs (slabs CS3, CS5, and CS6). Owing to the model limitations, concrete spalling was not considered in this study. Note that, the concrete spalling could result in the rapid loss of concrete cross-section and higher temperature of the inner concrete and reinforcement, i.e., the low load-carrying capacity (small fire resistance) and larger irrecoverable deflection.

5.1 Numerical model

The modelling of fire behaviour of the slab included two stages: thermal analysis and structural analysis. The temperatures of each span from thermal analysis were used as input data for the structural analysis of the slabs in fire. In the Vulcan software, the

complex behaviour of concrete and steel at elevated temperatures are considered. Both geometric and material nonlinearity of RC slab in fire are modelled. In this study, two concrete material models of EC2 and Lie' models [18] were used for comparison.

5.1.1 Thermal analysis model

In this study the Vulcan program [18] was used to predict the temperature of tested slabs. During the heating stage, the thermal properties of the concrete were calculated using the lower bound laws proposed in EC2 [35]. During the cooling phase, the thermal conductivity of concrete at the maximum temperature were not reversible during cooling, but the specific heat and density were reversible. A total number of 20 rectangular (four-node) elements were applied in layers (Fig. 15(a)) to predict the temperature distribution along the thickness of each slab. It is well known that the heat transfer between fire and slab surface is more complicated. The resultant emissivity associated with radiation is dependent on many factors, including the flame types, the compartment walls and the slab itself [36-37]. For instance, as discussed in Ref. [23, 36-38], for radiation heat transfer the resultant average emissivity was varied between 0 and 0.9, and for convection heat transfer the convection coefficient was ranged from 4 to 25 W/(m^2· K) in the thermal analysis. Hence in this study for the fire exposed and unexposed surface of the slab, the convection coefficient h_c, was assumed to be 10 and 5 W/(m^2 K), and the resultant average emissivity, ε_r, was assumed to be 0.3 and 0.2.

5.1.2 Concrete and steel constitutive models

The mechanical properties of steel and concrete in EC2 [35] were adopted during the heating and cooling stages. During the cooling phase, the free thermal strains of concrete and steel were reversible, and the transient strain was not considered. In addition, the stress-strain curves of the concrete during the cooling phase were dependent on the observed maximum temperature, but the stress-strain curves of the steel were equivalent to those in the heating phase.

5.1.3 Element meshes and layers

In the structural analysis, the cross-section of the slab was subdivided into 12 layers (Fig. 15(b)). As shown in Figs. 15(c) and 15(e), nine-node thick plate elements (Gauss or Integration points: G1-G9) were used, and the meshes were 14×7. The geometric non-linearity of the slab was taken into account.

612 *5.2 Model verification*

613 *5.2.1 Temperature prediction*

614 Figures 16(a)–(c) show comparisons of the predicted and measured concrete
615 temperatures in the slabs. In general, there was reasonable agreement between the
616 predicted and measured temperatures for all slabs during both the heating and cooling
617 stages. Ultimately, the model simulated the observed temperatures of the tested slabs.

618 *5.2.2 Deflection prediction*

619 The predicted mid-span deflection of each span was compared with the experimental
620 results, as shown in Figs. 17(a)–(c). During the heating stage, the predicted deflections
621 were in good agreement with the experimental results. However, during the cooling
622 stage, for slabs CS3 and CS5, there were larger discrepancies (earlier deflection
623 reversal) between the experimental and predicted results. In addition, a slope
624 discontinuity occurred in the predicted deflection-time curves for some spans as a result
625 of the deflection recovery (decreased temperature) of the adjacent spans. That is, once
626 the edge span began to cool and the adjacent slabs started to heat, additional
627 compression was induced in the cooling edge span, thereby increasing its vertical
628 displacement. This difference in the predicted result was attributed to the fact that the
629 entire expanding thermal strain (i.e., compression) was compensated for by the
630 mechanical strain in the concrete model, as the transient strain was implicitly
631 incorporated in the concrete model. In addition, as the transient thermal strain in the
632 EC2 model was recovered during the cooling stage, the initial elastic modulus used for
633 unloading was underestimated [20-21]. In this case, the implicit models slowly released
634 the stresses during cooling. Overall, the EC2 model, which includes implicitly the
635 transient strain, can be used to predict the behaviour of concrete slabs subjected to the
636 heating stage or uniform fire case (Slab CS6), but it may not be adapted for the cooling
637 phase.

638 Figs. 17(a)–(c) also show the predicted results using different thermal strain models for
639 the concrete [33, 35] shown in Fig. 15(d). During the heating and cooling stages, the
640 greater the thermal strain of the concrete was, the larger the residual deflections were,
641 owing to the larger internal forces. This observation is similar to the conclusion in
642 reference [23]. Using slab CS3 as an example, Figs. 18(a) and 18(b) show the bending
643 moment at Gauss point G5 of each element (Elements 43–56) as predicted by the EC2

and Lie thermal strain models, respectively. For instance, at 90, 180 and 270 minutes, the maximum bending moment of span A was -312.8, -161.2 and -35.4 N·m, respectively, as predicted by the EC2 model. Similarly, at 90, 180 and 270 minutes, the maximum moment of span A was -103.9, 243.6 and 317.1 N·m, respectively, as predicted by the Lie model. The large difference between the two predicted moments indicates clearly that the concrete thermal strain had a considerable effect on the internal force development of the concrete slabs subjected to the travelling fire.

In the practical application or a performance-based design, the structural fire engineers consider the actual behaviour (such as the forces redistribution and the collapse) of one structure and the accurate residual load bearing capacity of a building after the uniform or traveling fire [34]. When it comes to performance-based design, more accurate models should probably be used, and notably the concrete transient creep strain should be properly modelled with an explicit term. Otherwise, this implicit approach overestimates or underestimates permanent deformation and produces unrealistic response during the cooling phase of the traveling fire.

In fact, as discussed in Refs. [39-40], the new model is more accurate than EC2 model owing to the explicit calculation of concrete transient strain during the cooling phase of the fire. In addition, as discussed above, the spalling was not considered in this paper. Note that, the spalled concrete should be removed from the section of the slab, and the reduced concrete section and the new boundary surface should be considered in the subsequent time step for undertaking thermal and structural analysis [41]. Thus, in this paper, neglecting the spalling tends to overpredict the residual structural stiffness or recovery performance of the tested slabs during the cooling stage of fire.

6. Conclusions

In this study, six fire tests on three-span continuous reinforced concrete slabs subjected to travelling fires are presented. The non-linear finite element software, Vulcan, was used to predict the temperature and deflection of three continuous slabs without spalling. Based on the experimental results obtained in this study and the findings of references [13-14], the following conclusions can be drawn:

(1) According to conventional temperature failure criteria, earlier failure (i.e., lower fire resistance) easily occurs in the later heated spans of the continuous slab as a result of preheating. In addition, for the smaller thickness values, the detrimental effect of the

travelling fire scenario (i.e., fire spread direction and time delay) on the fire resistance of the slab will be greater. Therefore for the normal structural fire engineering design the detrimental effects of smaller thickness of floor slab need to be carefully considered.

(2) The concrete age and boundary conditions are two important factors that influence the occurrence of concrete spalling. When the concrete age is greater than two years, the spalling of a continuous slab subjected to any uniform or travelling fire scenario can be neglected. However, if the concrete age is less than half year, particularly the slab with high boundary restraint, the spalling should be considered.

(3) As the span-thickness ratio increases or the thickness decreases, the applied load has an important effect on the deflection trend in each span in the continuous slab, particularly the edge span. Thus, conventional deflection failure criterion should include the influence of the span-thickness ratio, thickness, applied load, and boundary conditions for edge and middle spans.

(4) In terms of the deflection failure criterion for the edge span, the uniform or travelling fire scenario can be considered as the worst fire case, as its maximum deflection is mainly dependent on the maximum temperature, heating duration, and applied load. However, for the middle span, several different fire scenarios should be analysed and compared to identify the worst fire case.

(5) The EC2 constitutive model may be not suitable for predicting the deflection in concrete slabs during the cooling phase, particularly in travelling fire scenarios.

Acknowledgements

This research was supported by National Natural Science Foundation of China (Grant No. 51408594 and 51808129), Key Projects of Fire Rescue Bureau of Emergency Management Department (Grant No. 2020XFZD14) and Jiangsu Key Laboratory of Environmental Impact and Structural Safety in Engineering (KFJJ202001). The authors gratefully acknowledge this support.

References

[1] Lim L, Wade C. Experimental fire tests of two-way concrete slabs. Fire engineering research report 02/12. New Zealand: University of Canterbury and BRANZ Ltd; 2002.

[2] Bailey CG, Toh WS. Small-scale concrete slab tests at ambient and elevated temperatures. Eng Struct 2007; 29: 2775-91.

[3] Dong YL, Zhu CJ. Limit load carrying capacity of two-way slabs with two edges clamped and two edges simply supported in fire. J Struct Eng 2010; 137: 1182-92.
[4] Wang Y, Yuan GL, Huang ZH, et al. Experimental study on the fire behaviour of reinforced concrete slabs under combined in-plane and out-of-plane loads. Eng Struct 2016; 128: 316-32.
[5] Wang Y, Bisby LA, Wang TY, et al. Fire behaviour of reinforced concrete slabs under combined biaxial in-plane and out-of-plane loads. Fire Saf J 2018; 96: 27-45.
[6] Chen LG. The experimental research of reinforced concrete slab. PhD Thesis, Xi'an University of Architecture and Technology, Xi'an, China, 2004 (in Chinese).
[7] Gao LT, Dong YL, Yuan AM. Experimental investigation of the behaviour of continuous slabs of unbonded prestressed concrete with the end-middle spans under fire. J. Harbin Inst. Technol. 2009; 41: 179-82 (in Chinese).
[8] Yuan AM, Dong YL, Gao LT. Behavior of unbonded prestressed continuous concrete slabs with the middle and edge span subjected to fire in sequence. Fire Saf J 2013; 56: 20-9
[9] Hou XM, Zheng WZ, Kodur VKR. Response of unbonded prestressed concrete continuous slabs under fire exposure. Eng Struct 2013; 56: 2139-48.
[10] Yang ZN, Dong YL, Xu WJ. Fire tests on two-way concrete slabs in a full-scale multi-storey steel-framed building. Fire Saf J 2013; 58: 38-48.
[11] Wang Y, Dong YL, Li B, Zhou GC. A fire test on continuous reinforced concrete slabs in a full-scale multi-story steel-framed building. Fire Saf J 2013; 61:232-42.
[12] Li B, Dong Y, Lou YJ. A fire test of continuous panels in a full-scale steel-framed structure. Eng Mech 2015; 32:145-53 (in Chinese).
[13] Wang Y, Duan YK, Ma S, et al. Behaviour of continuous reinforced concrete floor slabs subjected to different compartment fires. Eng Struct 2019; 197: 109445.
[14] Wang Y, Wu JC, Huang ZH, et al. Experimental studies on continuous reinforced concrete slabs under single and multi-compartment fires with cooling phase. Fire Saf J 2020; 111: 102915.
[15] GB 50010-2010. Code for design of concrete structures. Beijing: China Architecture and Building Press, 2010 (in Chinese).
[16] Lim L, Buchanan A, Moss P, Franssen JM. Numerical modelling of two-way reinforced concrete slabs in fire. Eng Struct 2004; 26: 1081-91.
[17] Wang Y, Yuan GL, Huang ZH, et al. Modelling of reinforced concrete slabs in fire.

740 Fire Saf J 2018; 100: 171-85.
741 [18] Huang ZH. The behaviour of reinforced concrete slabs in fire. Fire Saf J 2010;
742 45:271-82.
743 [19] Khalaf J, Huang ZH. The bond behaviour of reinforced concrete members at
744 elevated temperatures. Fire Saf J 2019; 103: 19-33.
745 [20] Gernay T, Franssen JM. A plastic-damage model for concrete in fire: Applications
746 in structural fire engineering. Fire Saf J 2015; 71: 268-78.
747 [21] Gernay T, Franssen JM. A formulation of the Eurocode 2 concrete model at
748 elevated temperature that includes an explicit term for transient creep. Fire Saf J 2012;
749 51:1-9.
750 [22] Hawileh RA, Kodur VKR. Performance of reinforced concrete slabs under
751 hydrocarbon fire exposure. Tunn Undergr Sp Tech 2018; 77: 177-87.
752 [23] Hamzeh H, Mark FG. GFRP reinforced concrete slabs in fire: Finite element
753 modelling. Eng Struct 2019; 183: 1109-20.
754 [24] Jiang J, Li GQ. Parameters affecting tensile membrane action of reinforced
755 concrete floors subjected to elevated temperatures. Fire Saf J 2018; 96: 59-73.
756 [25] Rackauskaite E, Kotsovinos P, Jeffers A, Rein G. Computational analysis of
757 thermal and structural failure criteria of a multi-storey steel frame exposed to fire. Eng
758 Struct 2019; 180: 524-43.
759 [26] Law A, Stern-Gottfried J, Gillie M, Rein G. The influence of travelling fires on a
760 concrete frame. Eng Struct 2011; 33: 1635-42.
761 [27] Ellobody E, Bailey CG. Structural performance of a post-tensioned concrete floor
762 during horizontally travelling fires. Eng Struct 2011; 33: 1908-17.
763 [28] Jiang QY , Kotsovinos P , Usmani A , et al. Numerical investigation of thermal
764 responses of a composite structure in horizontally traveling fires using Opensees.
765 Procedia Engineering 2013: 62: 736-44.
766 [29] GB 50009-2001. Load code for the design of building structures. Beijing: China
767 Architecture and Building Press, 2006. (in Chinese).
768 [30] GB 50016-2014. Code for fire protection design of buildings. Beijing: China
769 Architecture and Building Press, 2018. (in Chinese).
770 [31] Ye Li, Kang Hai Tan, En-Hua Yang. Influence of aggregate size and inclusion of
771 polypropylene and steel fibers on the hot permeability of ultra-high performance
772 concrete (UHPC) at elevated temperature. Constr Build Mater, 2018, 169: 629-637.

[32] BSI. BS 476-3:1987 Fire tests on building materials and structures. Part 10. Method from Determination of the Fire Resistance of Elements of Construction (General Principles). UK, 1987.

[33] ASTM Standard Methods of Fire Test of Building Construction and Materials, American Society for Testing and Materials, West Conshohocken, PA, 2001, pp. E119-E201.

[34] Wang Y, Chen ZX, Jiang YQ, et al. Residual properties of three-span continuous reinforced concrete slabs subjected to different compartment fires. Eng Struct 2020; 208: 110352.

[35] E. 1992, BS EN 1992: Eurocode 2-Design of Concrete Structures-Part 1-2: General Rules Structural Fire Design; 2004.

[36] Tenchev R T, Li L Y, Purkiss J A, Khalafallah B H. Finite element analysis of coupled heat and mass transfer in concrete when it is in a fire. Mag Concr Res 2001; 53: 117-25.

[37] Lamont S, Usmani A S, Drysdale D D. Heat transfer analysis of the composite slab in the Cardington frame fire tests. Fire Saf J 2001; 36: 815-39.

[38] Daniel Di Capua, Antonio R. Mari. Nonlinear analysis of reinforced concrete cross-sections exposed to fire. Fire Saf J 2007; 42:139-49.

[39] Alogla S, Kodur V K R. Quantifying transient creep effects on fire response of reinforced concrete columns. Eng Struct 2018; 174: 885-95.

[40] Gernay T. Effect of transient creep strain model on the behavior of concrete columns subjected to heating and cooling. Fire Technol 2012; 48: 313-29.

[41] M.B. Dwaikat, V.K.R. Kodur. Hydrothermal model for predicting fire-indu ced spalling in concrete structural systems. Fire Saf J, 2009, 44: 425-434.

798 **Captions**

799 Fig.1 Details of the fire test (all dimensions in mm) (a) Reinforcement details; (b)
800 Photos of the furnace; (c) Plan view of the furnace; (d) Typical thermocouple layout;
801 (e) Sectional thermocouple layout across the depth of the slab; (f) Layout of vertical
802 and horizontal displacement transducers.
803 Fig. 2 Details of the loads and restrained beams (all dimensions in mm) (a) Photos of
804 the iron bricks and restrained beams at each corner; (b) Loading device, supports, and
805 corner restraints; (c) Position of the pressure sensor.
806 Fig. 3 Average furnace temperature-time curves for the six slabs (a) Slab CS1; (b) Slab
807 CS2; (c) Slab CS3; (d) Slab CS4; (e) Slab CS5; (f) Slab CS6
808 Fig. 4 Temperature distributions through the thickness of the six slabs (a) Slab CS1; (b)
809 Slab CS2; (c) Slab CS3; (d) Slab CS4; (e) Slab CS5; (f) Slab CS6
810 Fig. 5 Reinforcing steel temperatures in the six slabs (a) Slab CS1; (b) Slab CS2; (c)
811 Slab CS3; (d) Slab CS4; (e) Slab CS5; (f) Slab CS6
812 Fig. 6 Vertical displacement-time curves for the six slabs (a) Slab CS1; (b) Slab CS2;
813 (c) Slab CS3; (d) Slab CS4; (e) Slab CS5; (f) Slab CS6
814 Fig. 7 Vertical displacement-average furnace temperature curves for the six slabs (a)
815 Slab CS1; (b) Slab CS2; (c) Slab CS3; (d) Slab CS4; (e) Slab CS5; (f) Slab CS6.
816 Fig. 8 Horizontal displacement-time curves for the six slabs (a) Slab CS1; (b) Slab CS2;
817 (c) Slab CS3; (d) Slab CS4; (e) Slab CS5; (f) Slab CS6
818 Fig. 9 Failure modes of Slab CS1: (a) cracking pattern on the top surface; (b) crack
819 development; (c) bottom surface; and (d) cracking pattern on the bottom surface
820 Fig. 10 Failure modes of Slab CS2: (a) cracking pattern on the top surface; (b) crack
821 development; (c) bottom surface; and (d) cracking pattern on the bottom surface
822 Fig. 11 Failure modes of Slab CS3: (a) cracking pattern on the top surface; (b) crack
823 development; (c) bottom surface; and (d) cracking pattern on the bottom surface
824 Fig. 12 Failure modes of Slab CS4: (a) cracking pattern on the top surface; (b) crack
825 development; (c) bottom surface; and (d) cracking pattern on the bottom surface
826 Fig. 13 Failure modes of Slab CS5: (a) cracking pattern on the top surface; (b) crack
827 development; (c) bottom surface; and (d) cracking pattern on the bottom surface
828 Fig. 14 Failure modes of Slab CS6: (a) cracking pattern on the top surface; (b) crack
829 development; (c) bottom surface; and (d) cracking pattern on the bottom surface
830 Fig. 15 Temperature and structural models of the tested slabs (dimensions in mm) (a)

Figure 1

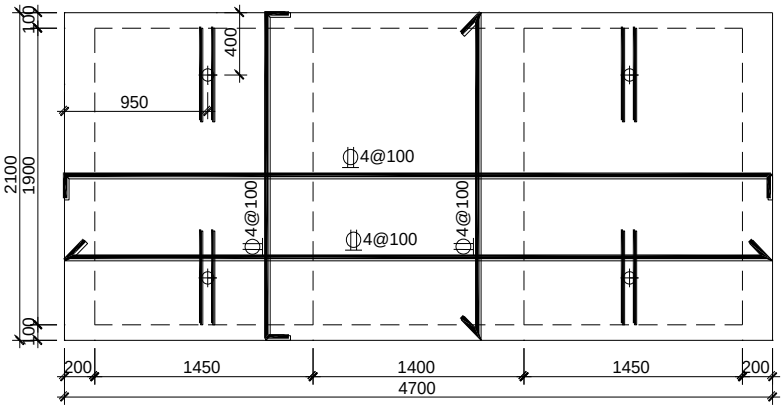

(a) Reinforcement details

(b) Photos of the furnace

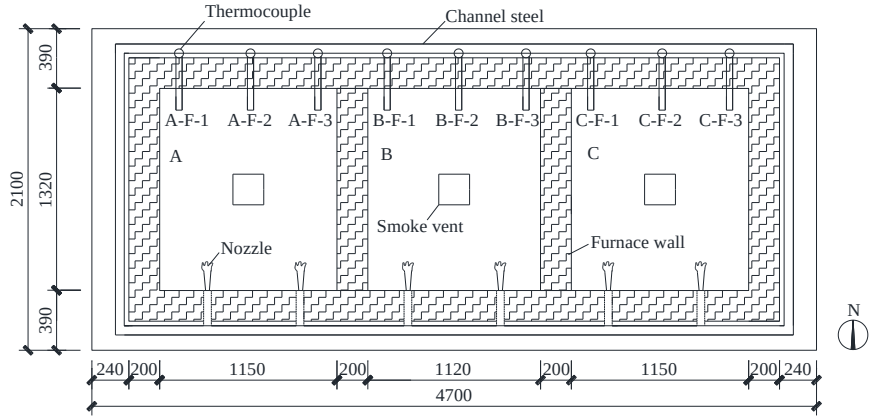

(c) Plan view of the furnace

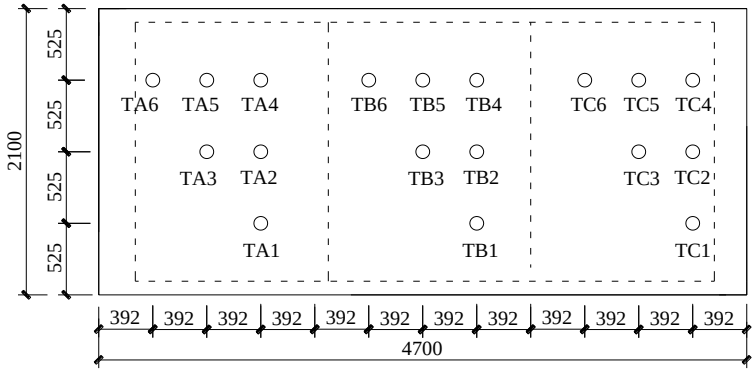

(d) Typical thermocouple layout

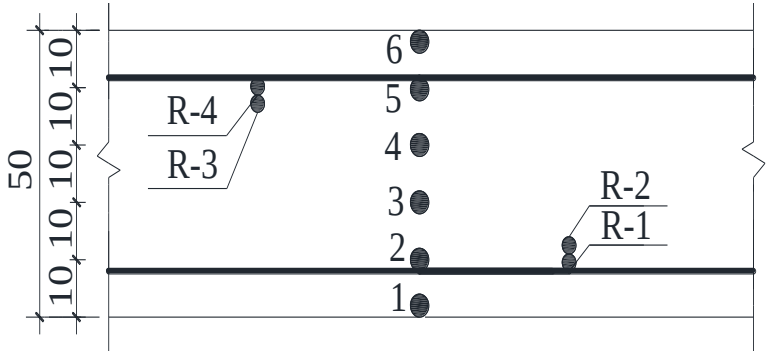

(e) Sectional thermocouple layout across the depth of the slab

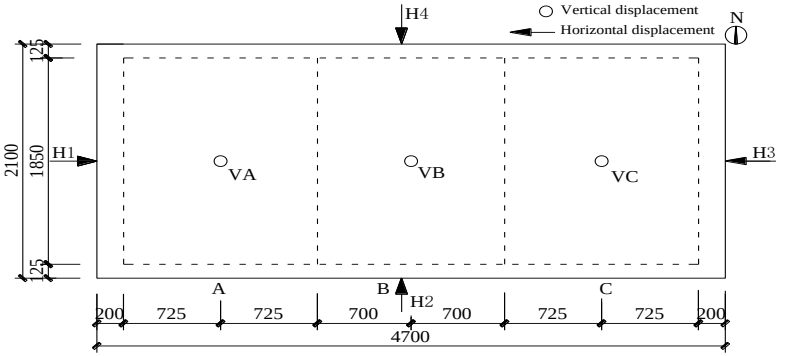

(f) Layout of vertical and horizontal displacement transducers

Fig.1 Details of the fire test (all dimensions in mm) (a) Reinforcement details; (b) Photos of the furnace; (c) Plan view of the furnace; (d) Typical thermocouple layout; (e) Sectional thermocouple layout across the depth of the slab; (f) Layout of vertical and horizontal displacement transducers.

Figure 2

(a) Photos of the iron bricks and restrained beams at each corner

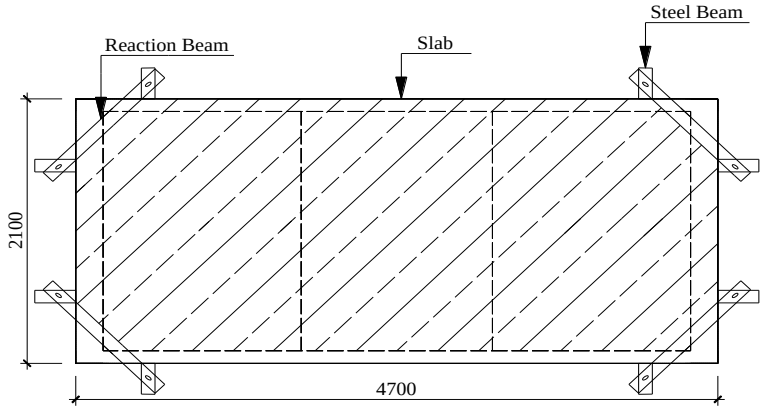

(b) Loading device, supports, and corner restraints

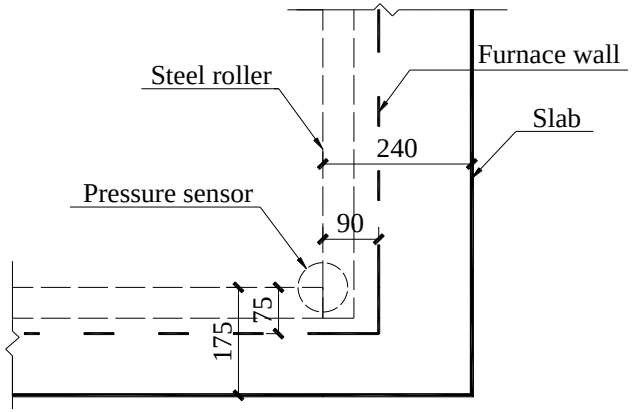

(c) Position of the pressure sensor

Fig. 2 Details of the loads and restrained beams (all dimensions in mm) (a) Photos of the iron bricks and restrained beams at each corner; (b) Loading device, supports, and corner restraints; (c) Position of the pressure sensor.

Figure 3

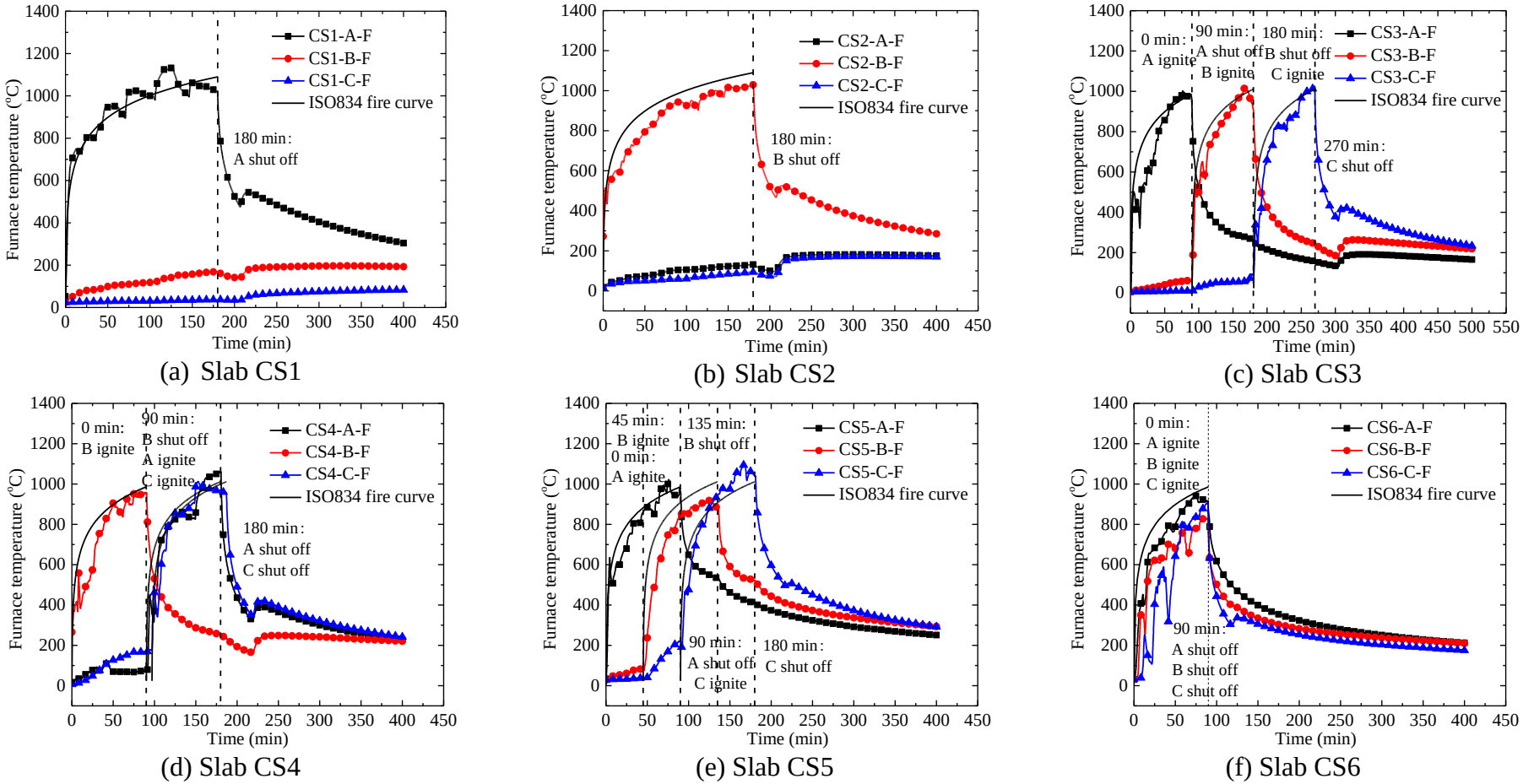

Fig. 3 Average furnace temperature-time curves for the six slabs

Figure 4

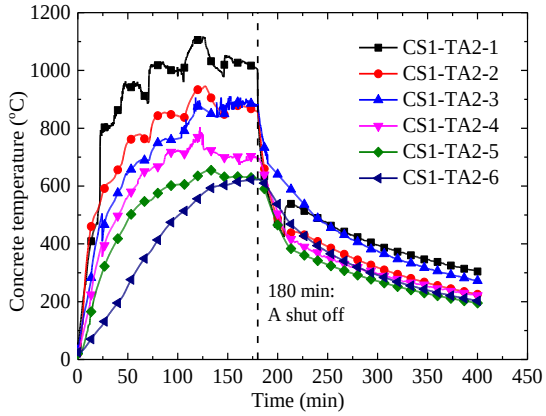

Compartment CS1-A

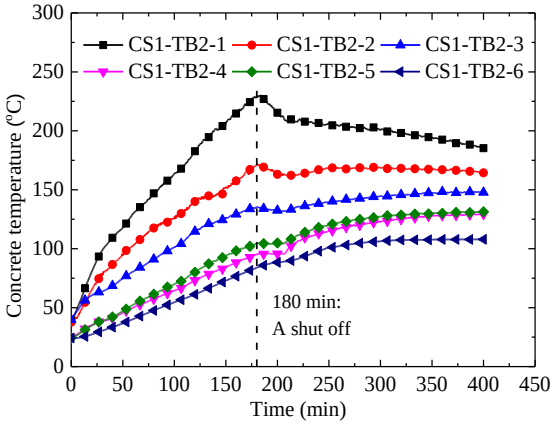

Compartment CS1-B

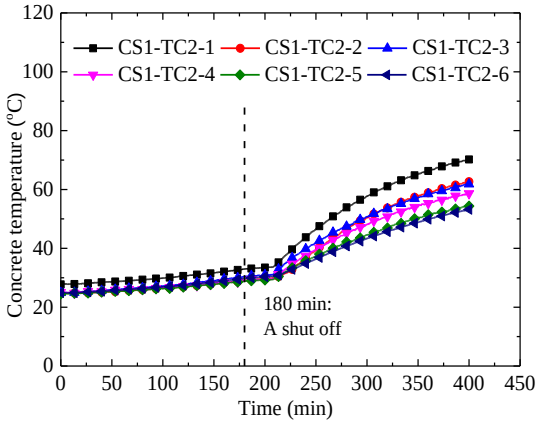

Compartment CS1-C

(a) Slab CS1

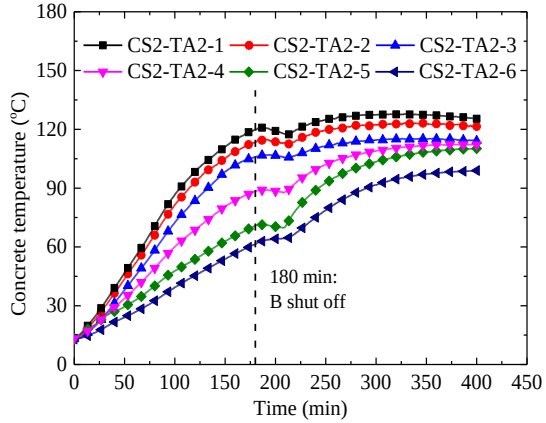

Compartment CS2-A

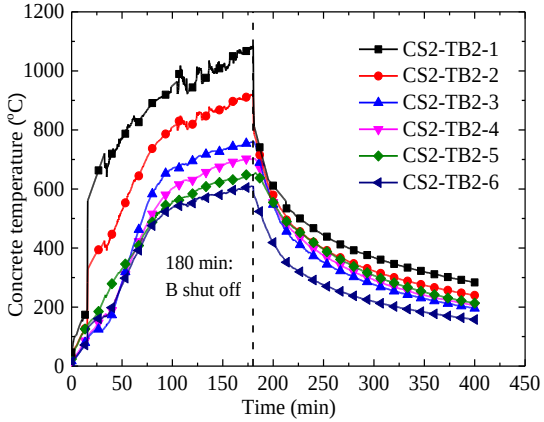

Compartment CS2-B

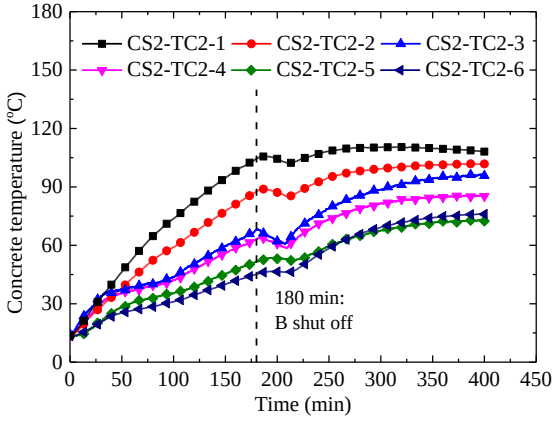

Compartment CS2-C

(b) Slab CS2

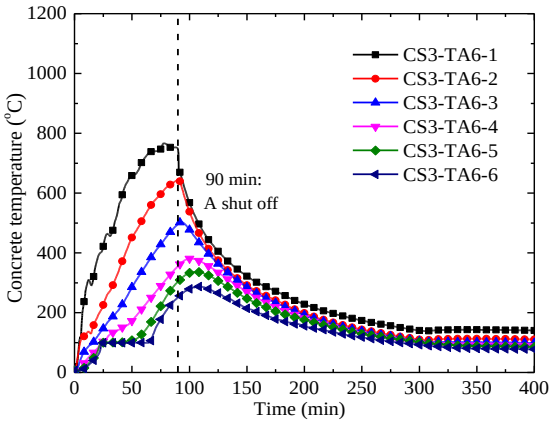

Compartment CS3-A

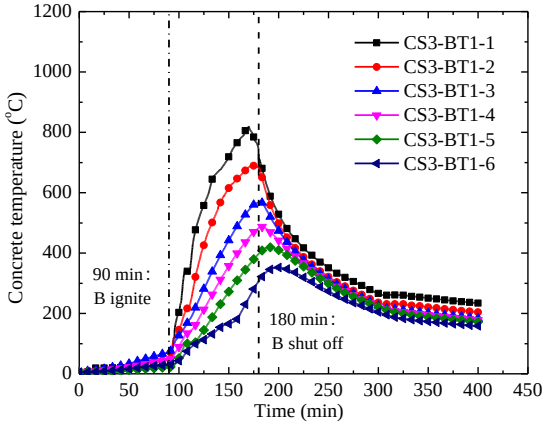

Compartment CS3-B

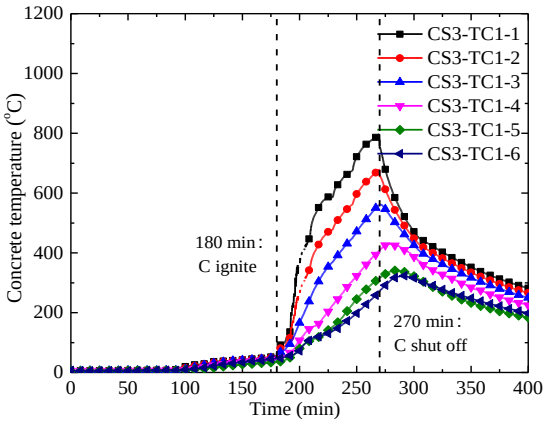

Compartment CS3-C

(c) Slab CS3

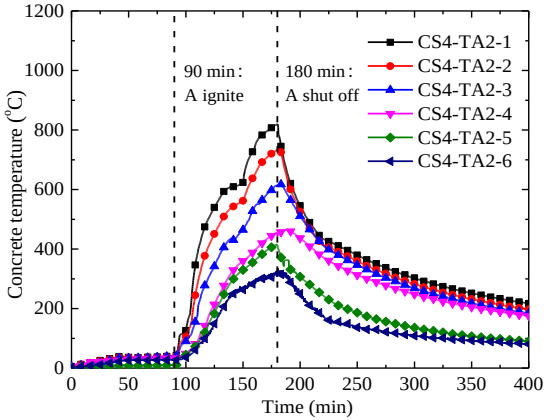

Compartment CS4-A

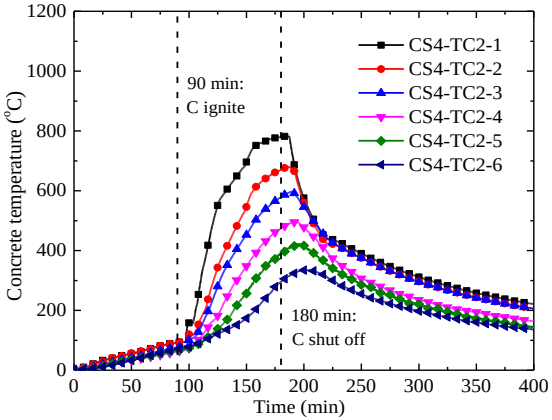

Compartment CS4-C

(d) Slab CS4

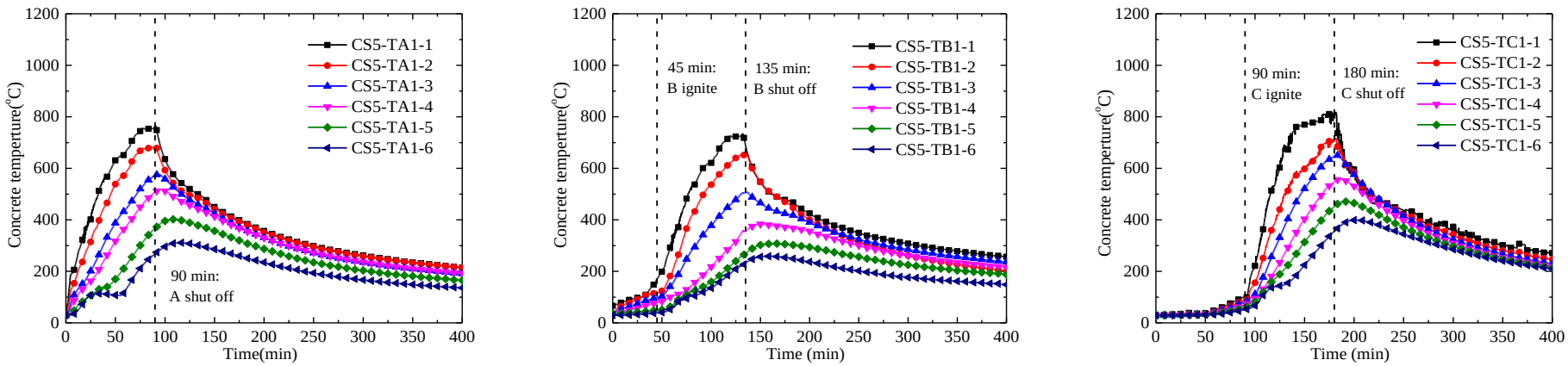

(e) Slab CS5

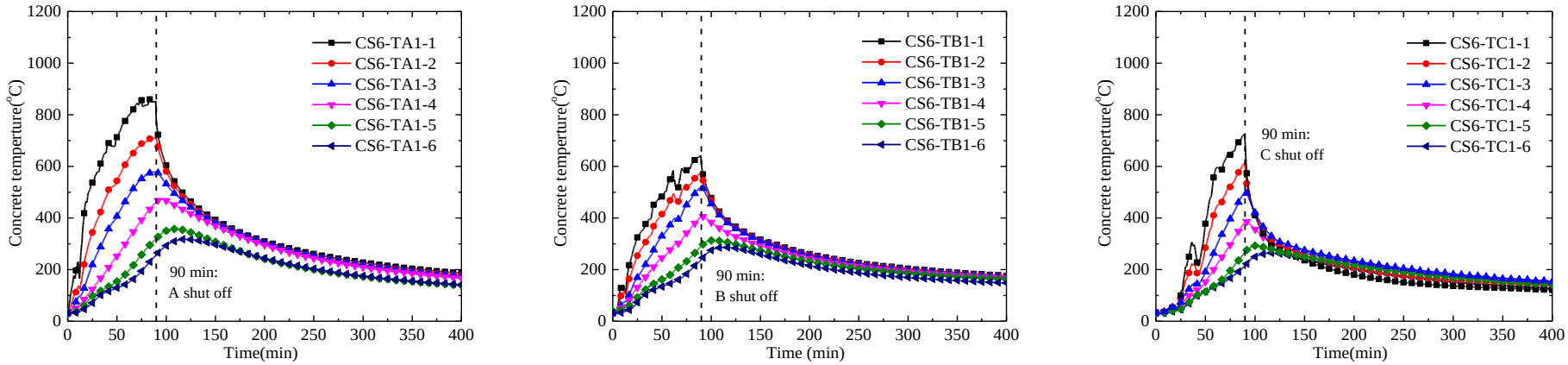

(f) Slab CS6

Fig. 4 Temperature distributions through the thickness of the six slabs

Figure 5

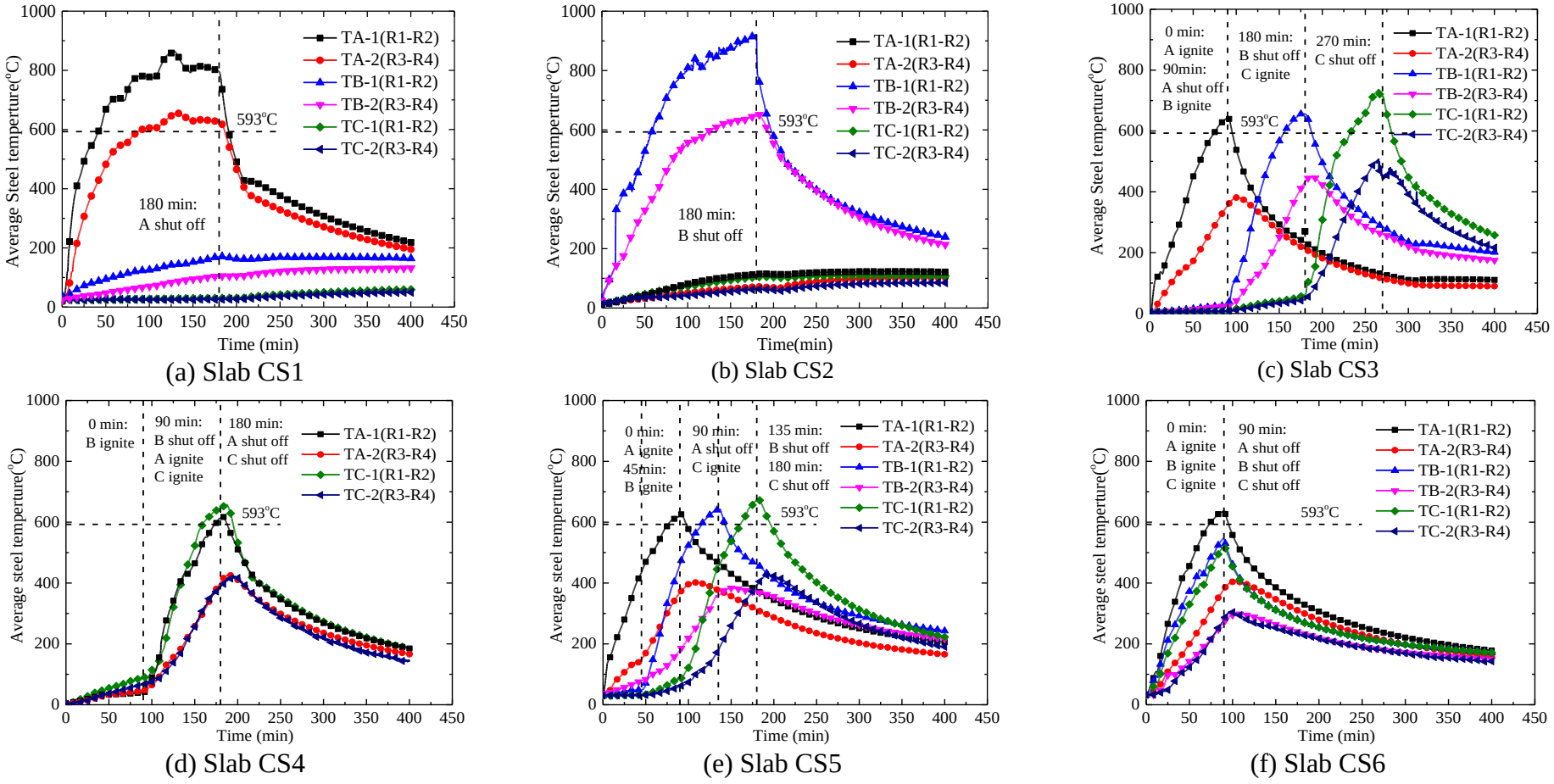

Fig. 5 Reinforcing steel temperatures in the six slabs

Figure 6

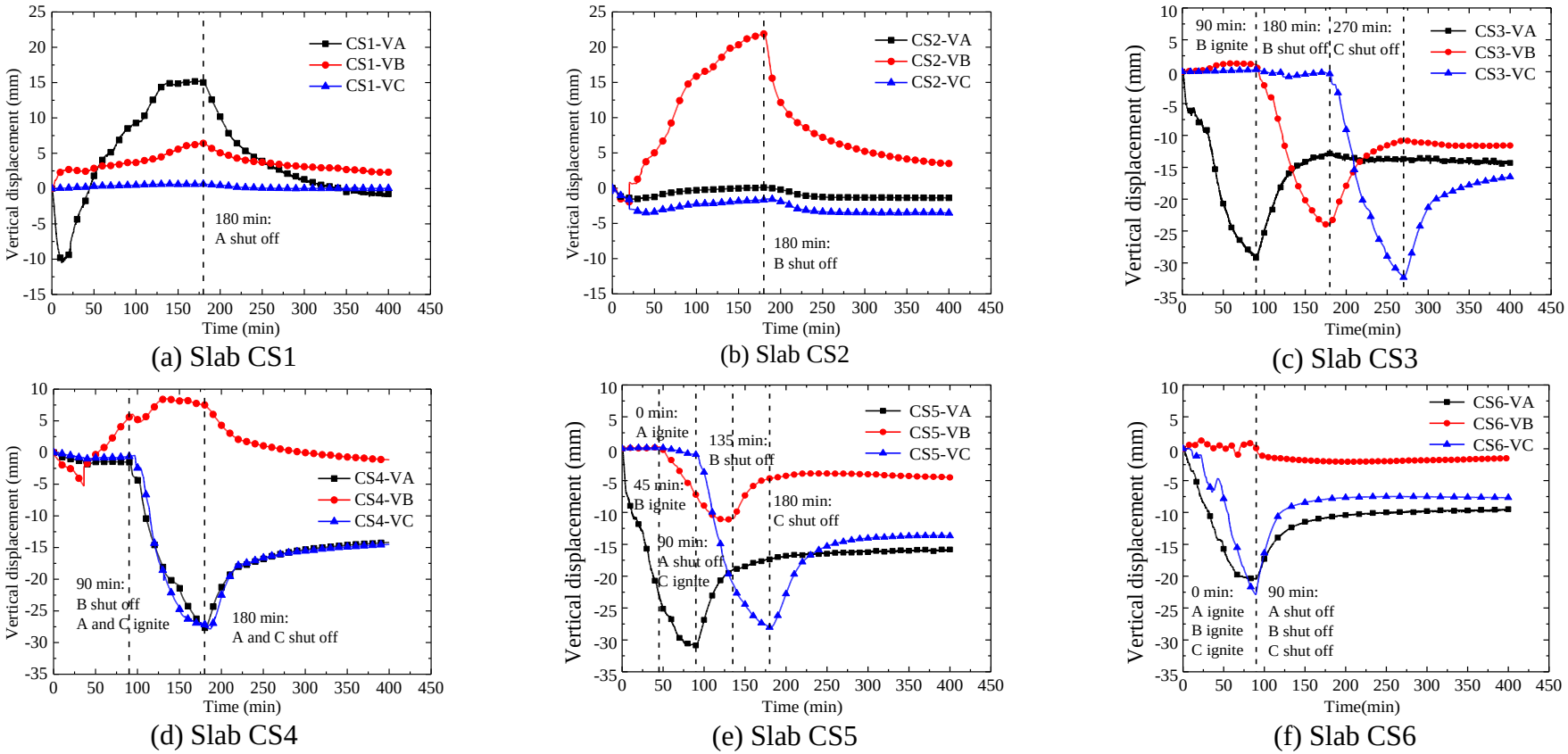

Fig. 6 Vertical displacement-time curves for the six slabs

Figure 7

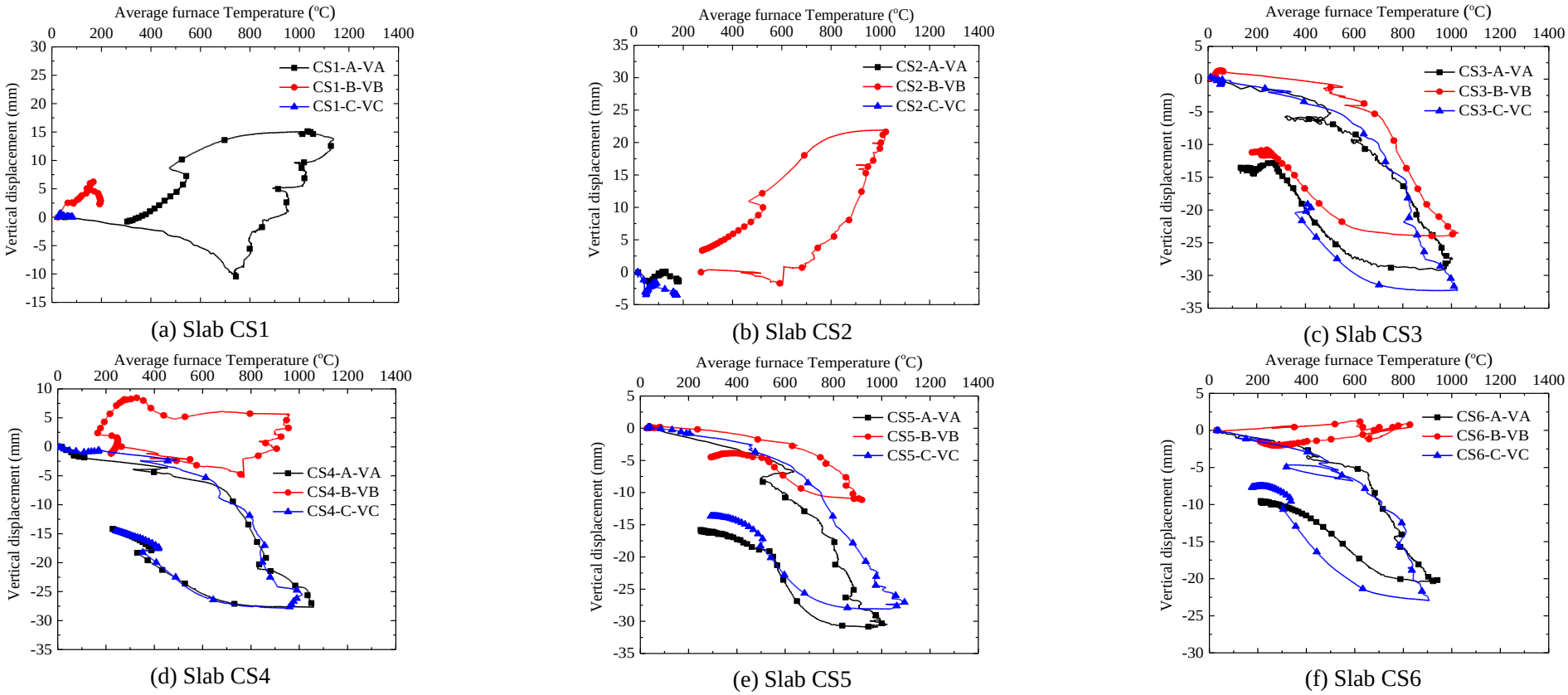

Fig. 7 Vertical displacement-average furnace temperature curves for the six slabs

Figure 8

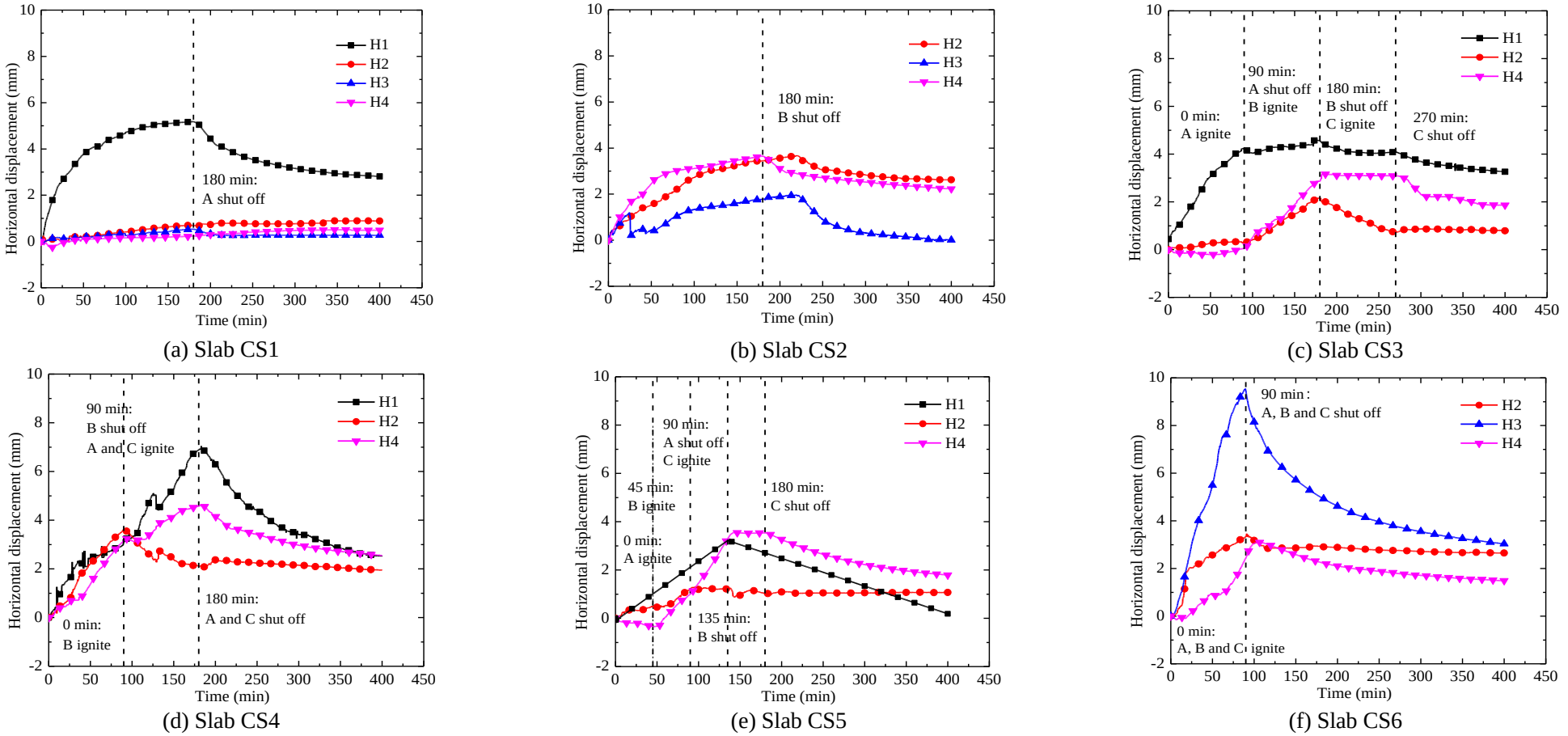

Fig. 8 Horizontal displacement-time curves for the six slabs

Figure 9

(a) Cracking pattern on the top surface

(c) Bottom surface

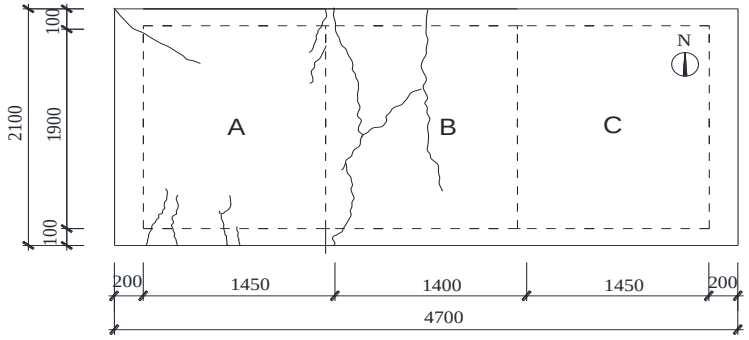

(b) Crack development during the test

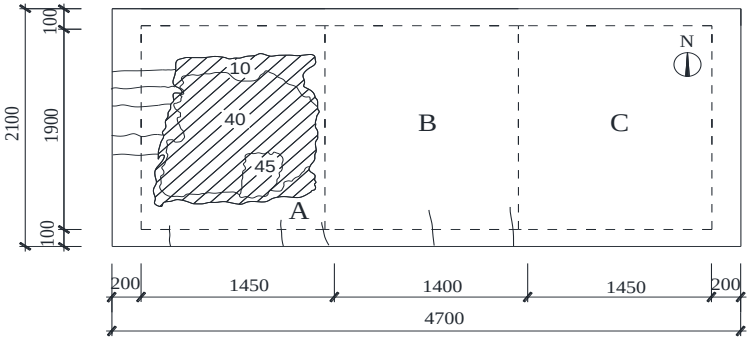

(d) Cracking pattern on the bottom surface

Fig. 9 Failure modes of Slab CS1: (a) cracking pattern on the top surface, (b) crack development, (c) bottom surface, and (d) cracking pattern on the bottom surface

Figure 10

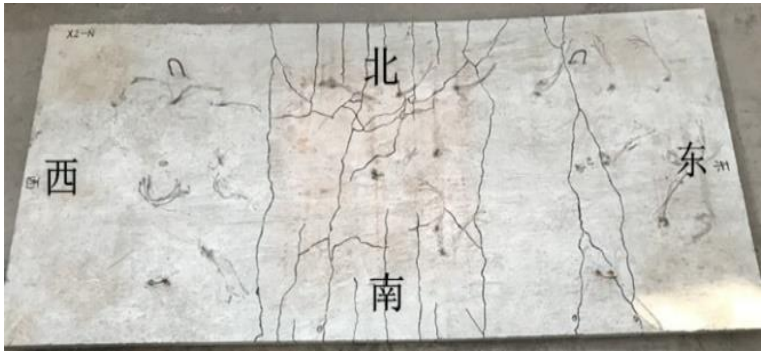

(a) Cracking pattern on the top surface

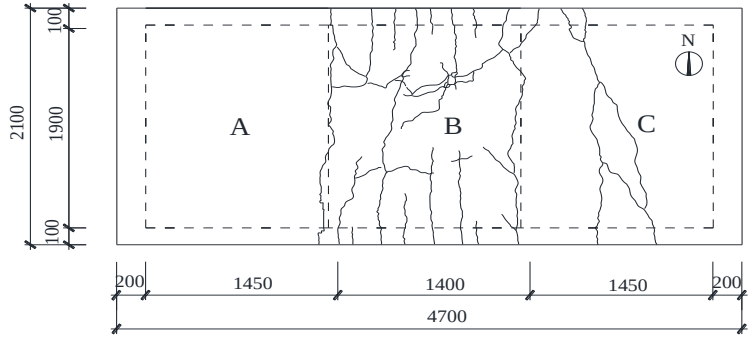

(b) Crack development during the test

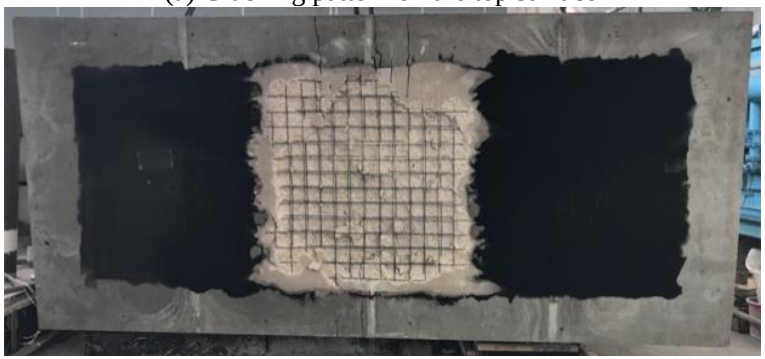

(c) Bottom surface

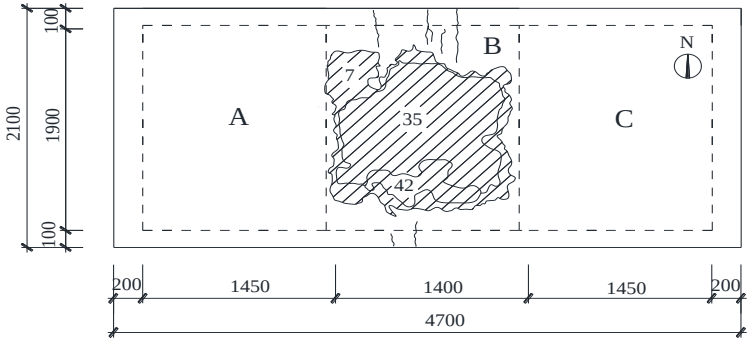

(d) Cracking pattern on the bottom surface

Fig. 10 Failure modes of Slab CS2: (a) cracking pattern on the top surface, (b) crack development, (c) bottom surface, and (d) cracking pattern on the bottom surface

Figure 11

(a) Cracking pattern on the top surface

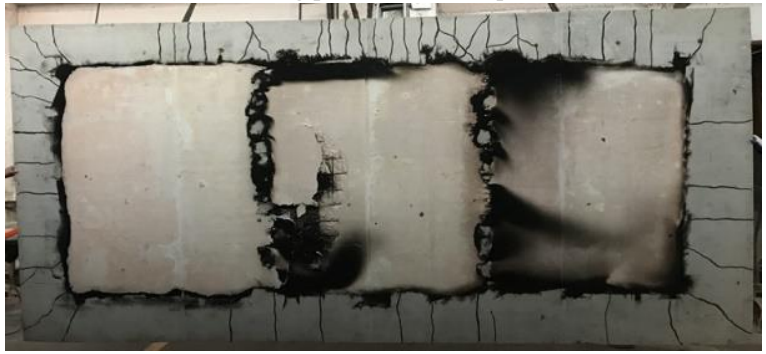

(c) Bottom surface

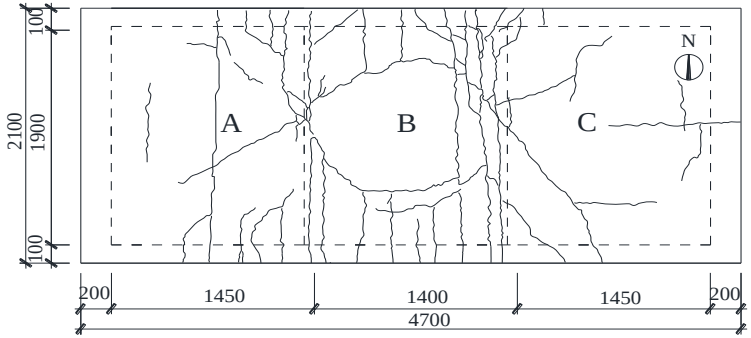

(b) Crack development during the test

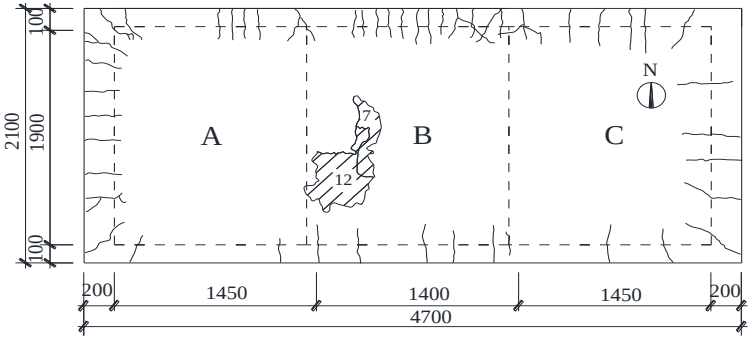

(d) Cracking pattern on the bottom surface

Fig. 11 Failure modes of Slab CS3: (a) cracking pattern on the top surface, (b) crack development, (c) bottom surface, and (d) cracking pattern on the bottom surface

Figure 12

(a) Cracking pattern on the top surface

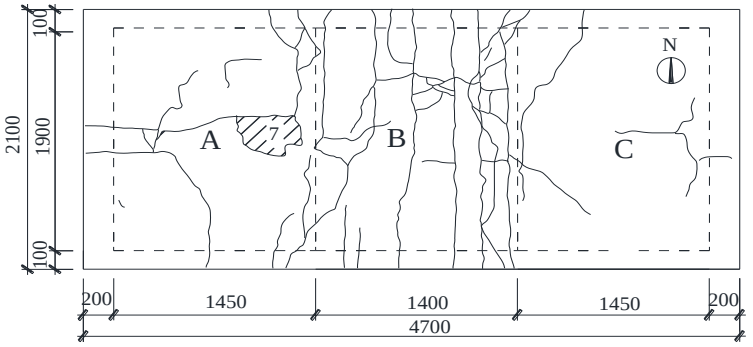

(b) Crack development during the test

(c) Bottom surface

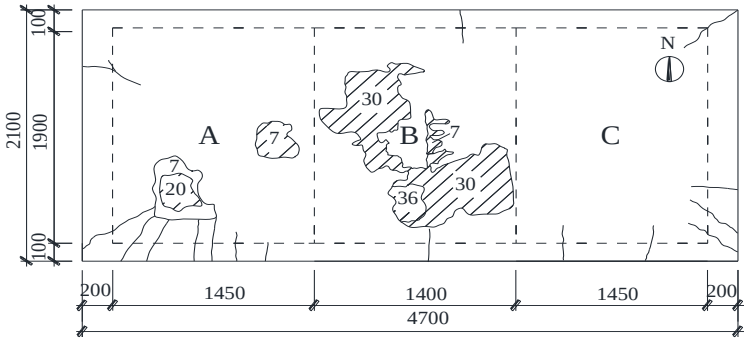

(d) Cracking pattern on the bottom surface

Fig. 12 Failure modes of Slab CS4: (a) cracking pattern on the top surface, (b) crack development, (c) bottom surface, and (d) cracking pattern on the bottom surface

Figure 13

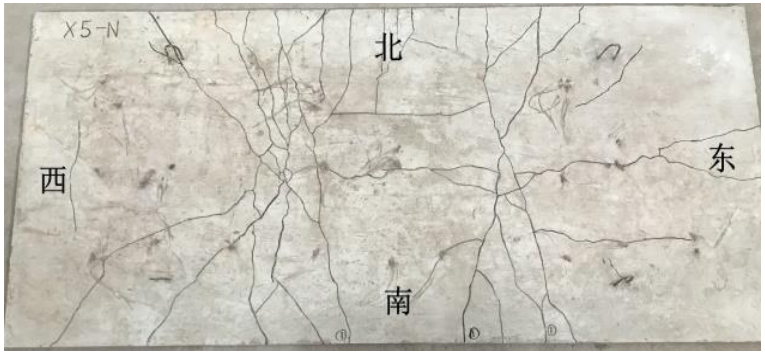

(a) Cracking pattern on the top surface

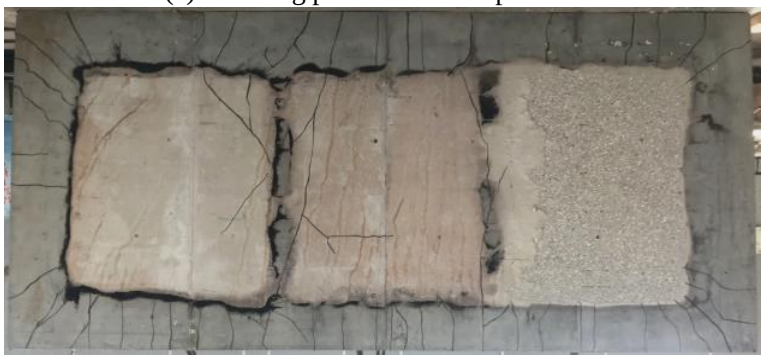

(c) Bottom surface

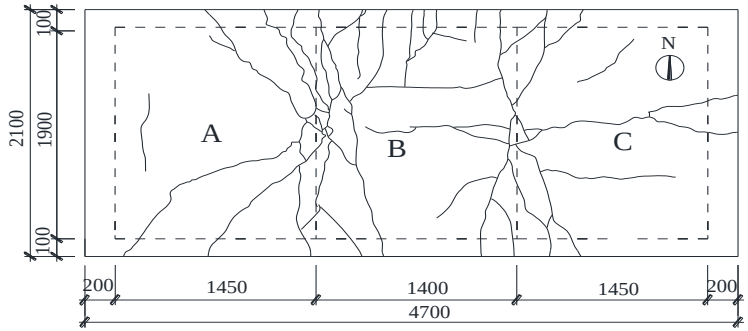

(b) Crack development during the test

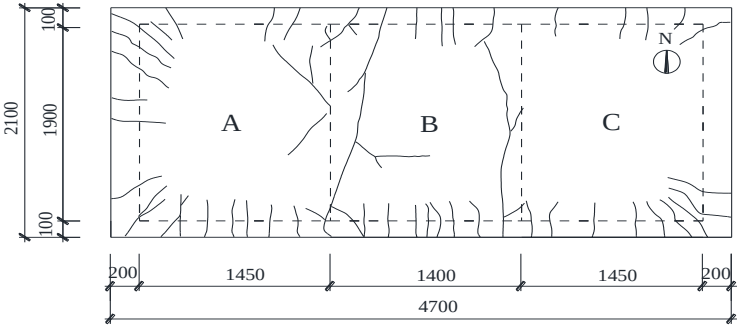

(d) Cracking pattern on the bottom surface

Fig. 13 Failure modes of Slab CS5: (a) cracking pattern on the top surface, (b) crack development, (c) bottom surface, and (d) cracking pattern on the bottom surface

Figure 14

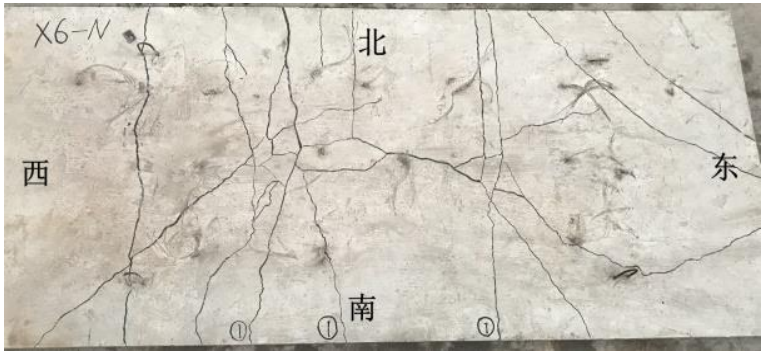

(a) Cracking pattern on the top surface

(c) Bottom surface

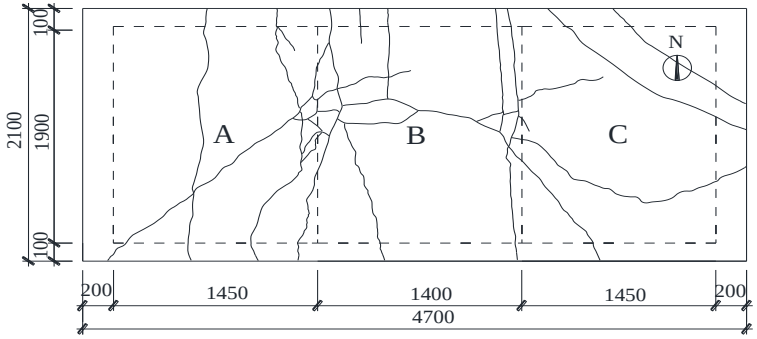

(b) Crack development during the test

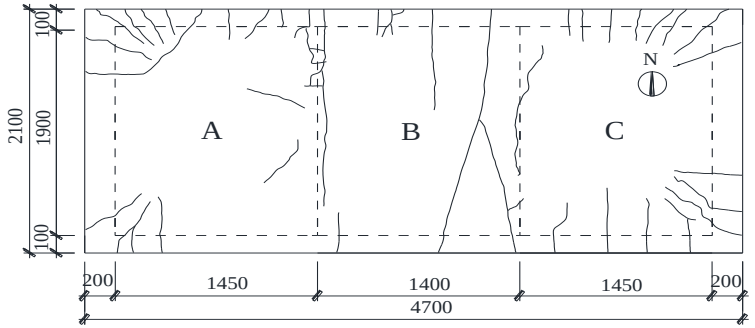

(d) Cracking pattern on the bottom surface

Fig. 14 Failure modes of Slab CS6: (a) cracking pattern on the top surface, (b) crack development, (c) bottom surface, and (d) cracking pattern on the bottom surface

Figure 15

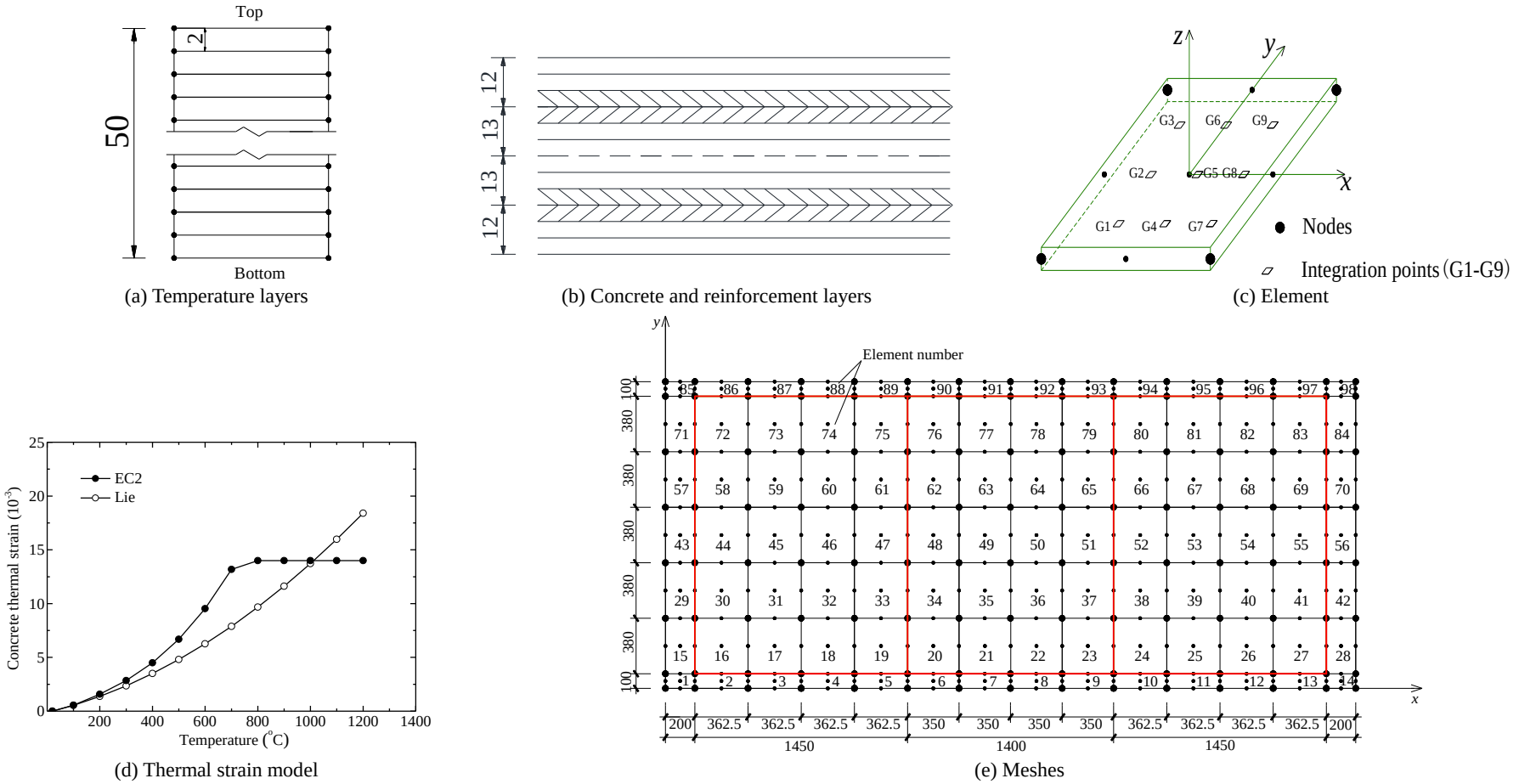

(a) Temperature layers

(b) Concrete and reinforcement layers

(c) Element

(d) Thermal strain model

(e) Meshes

Fig. 15 Temperature and structural models of the tested slabs (dimensions in mm)

Figure 16

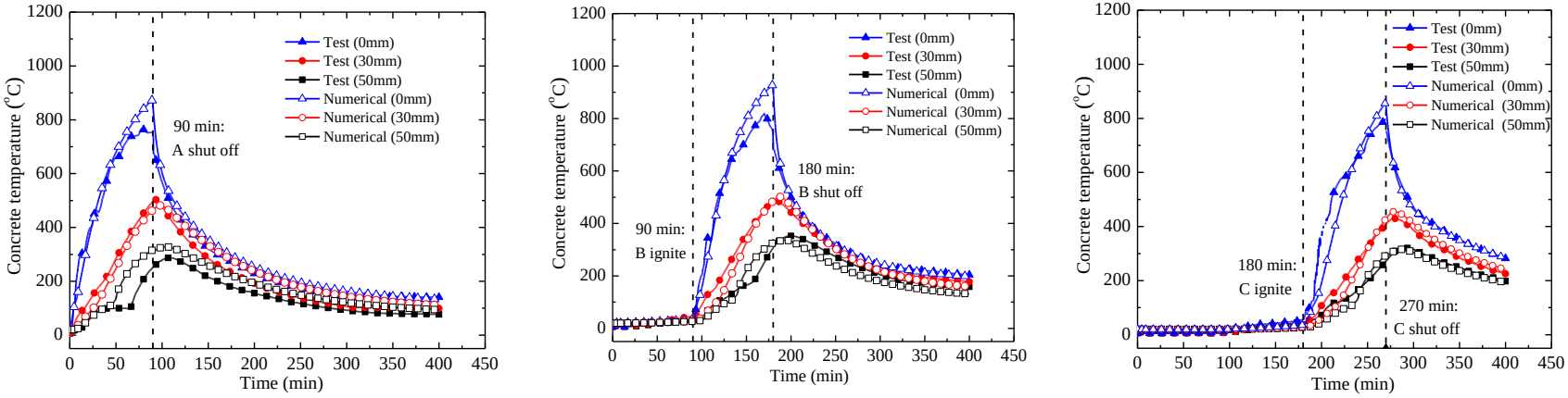

Span CS3-A Span CS3-B Span CS3-C

(a) Slab CS3

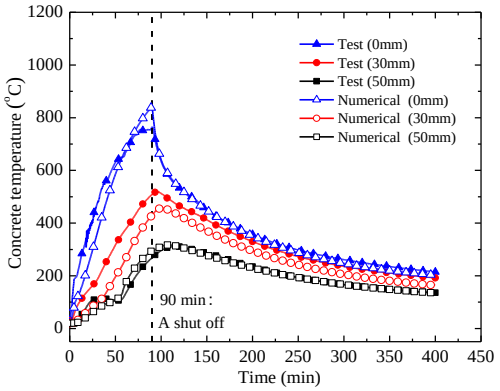

Span CS5-A

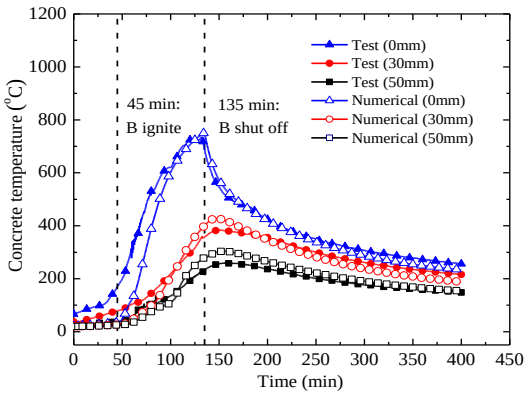

Span CS5-B

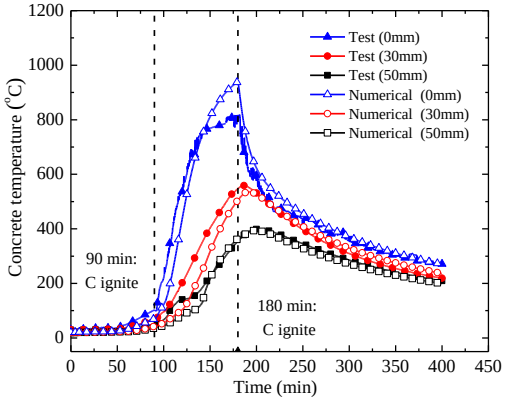

Span CS5-C

(b) Slab CS5

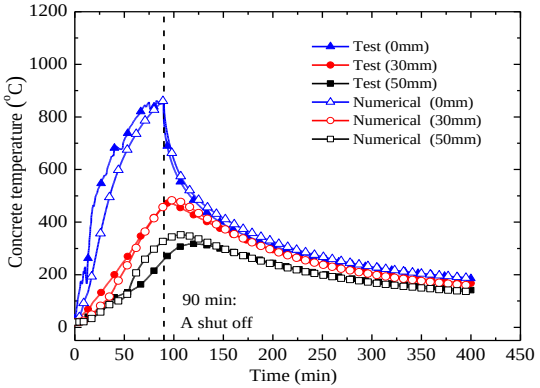

Span CS6-A

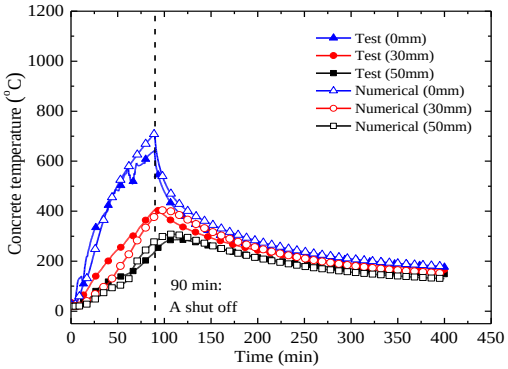

Span CS6-B

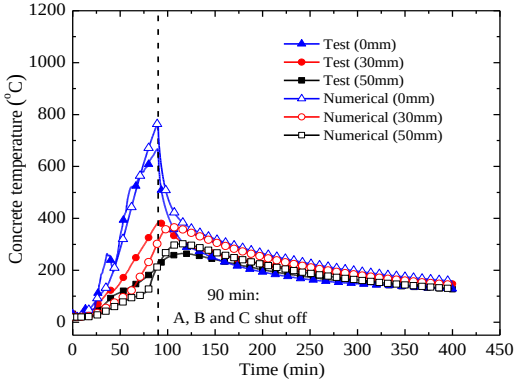

Span CS6-C

(c) Slab CS6

Fig. 16 Comparison of predicted and tested temperatures: (a) Slab CS3, (b) Slab CS5, and (c) Slab CS6

Figure 17

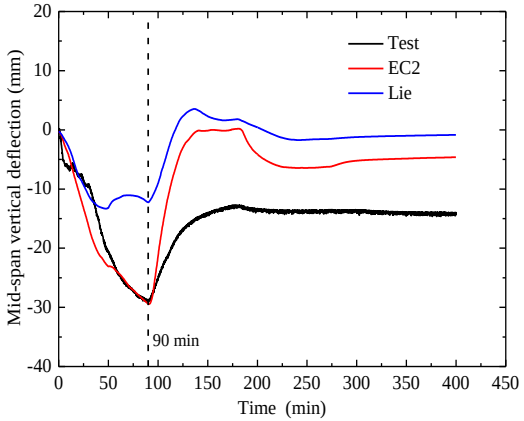

Span CS3-A

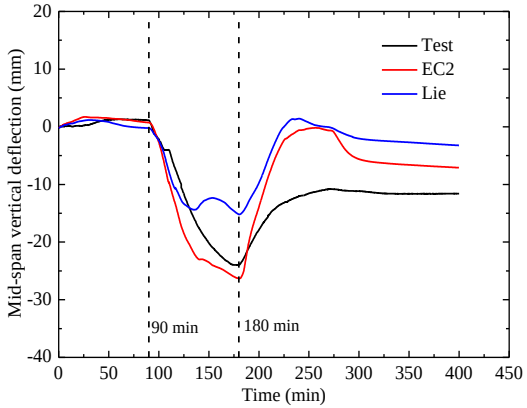

Span CS3-B

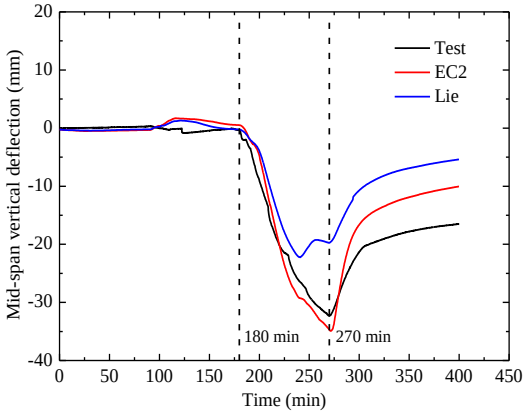

Span CS3-C

(a) Slab CS3

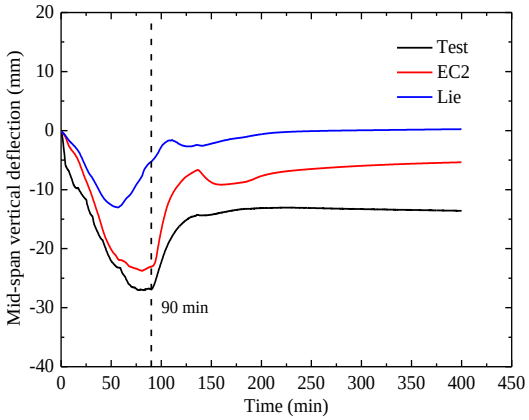

Span CS5-A

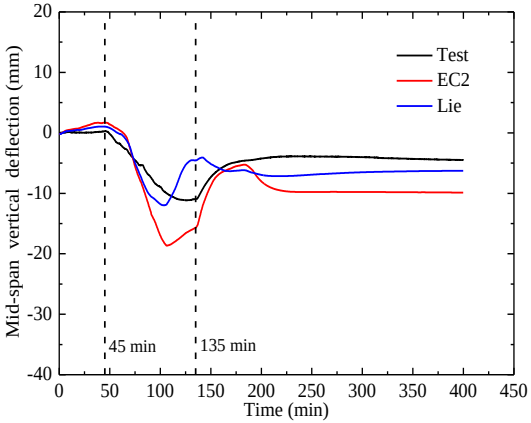

Span CS5-B

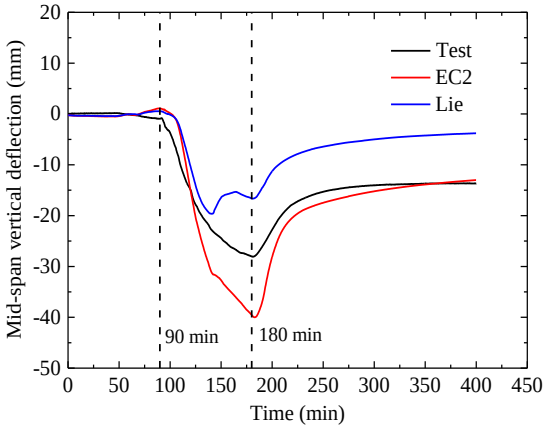

Span CS5-C

(b) Slab CS5

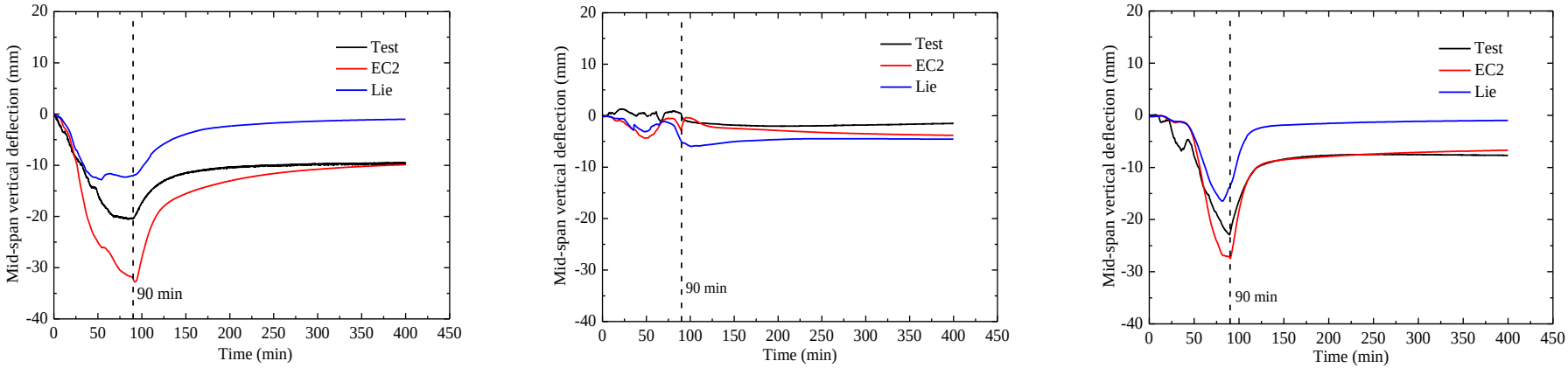

(c) Slab CS6

Fig. 17 Comparison of predicted and tested mid-span deflection-time curves: (a) Slab CS3, (b) Slab CS5, and (c) Slab CS6

Figure 18

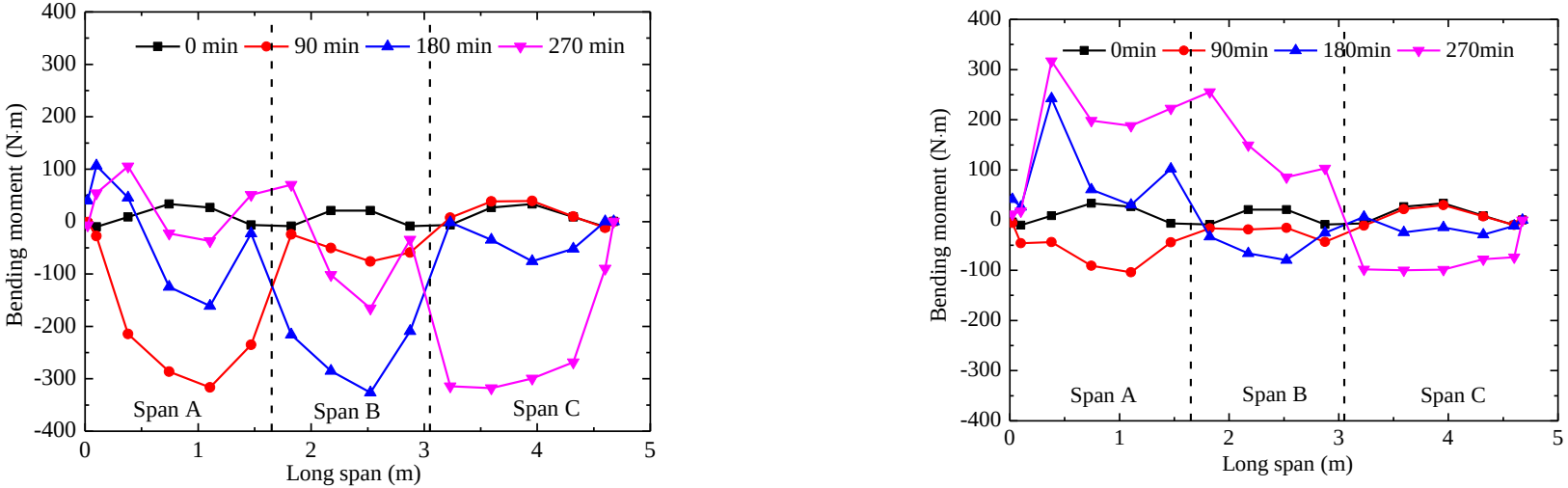

(a) EC2 model

(b) Lie model

Fig. 18 Comparison of bending moments predicted by EC2 and Lie thermal strain models (Slab CS3)

Tables:

Table 1 Mixing proportion of the concrete (kg/m^3)

Water	Cement	Sand	Coarse Aggregate (5-12mm)	Admixtures
185	240	557	1178	154

Table 2 Comparison of key parameters of the present slabs and the slabs in Refs. [13-14]

Parameter	Present slabs						Ref. [14]					Ref. [13]			
	CS1	CS2	CS3	CS4	CS5	CS6	S1	S2	S3	S4	S5	B1	B2	B3	B4
Days (d)	92	153	182	196	378	385	189	198	218	225	236	749	701	716	730
Fire scenario (min)	A (0,180)	B (0,180)	A (0, 90) → B (90, 180) and C (180, 270) *	B (0, 90) → A (0, 180) and C (180, 270)	A (0, 90) → B (45, 135) and C (90, 180)	A, B, and C (0, 90)	A (0, 190)	B (0, 200)	A and C (0, 160)	A and B (0, 180)	A, B and C (0, 180)	B (0, 180) →A (60, 235) and C (60, 235)	B (0, 160)→A (30, 160) and C (30, 160)	A (0, 180) →B (60, 240) → C (120, 300)	A (0, 180) →C (60, 240) → B (120, 300)
Total fire duration (min)	180	180	270	270	180	90	400	400	400	400	400	360	400	600	600
Concrete cover (mm)	8								10				15		
Thickness (mm)	50								80				100		
Reinforcing bars (mm)	4								6				8		
Characteristic cube strength of concrete (MPa)	34								40				30		
Load (kPa)	1.0	1.0	3.0	3.0	3.0	3.0			2.0				2.0		

* A (0, 90) →B (90, 180) and C (180, 270): 0 (90 and 180) represents the fire ignition time for Compartment A (B and C), 90 (180 and 270) represents the shut-off time for Compartment A (B and C). "→": fire spread direction

Table 3 Concrete and reinforcement temperatures of tested slabs at different times

Slab	Compartment	Furnace temperature (°C)			Concrete temperature (°C) at the shut-off time		Concrete temperature (°C) at the end of fire test		Maximum steel temperature (°C) at the shut-off time		Maximum steel temperature (°C) at the end of fire test		Maximum deflection during the heating stage (mm)	Residual deflection at the end of the test (mm)
		Maximum furnace temperature	Furnace temperature at the shut-off time	Furnace temperature at end of fire test	Bottom surface	Top surface	Bottom surface	Top surface	Bottom	Top	Bottom	Top		
CS1	A	1137	1009	303	926	623	304	193	794	626	218	197	15.0	-1.2
	B	196	169	192	229	84	186	108	171	104	165	132	6.4	2.3
	C	83	37	83	33	30	70	53	30	25	61	48	0.6	0
CS2	A	181	131	175	113	88	125	99	113	71	121	103	0.1	-1.4
	B	1030	1029	285	1085	610	283	153	916	647	236	211	21.9	3.4
	C	173	93	170	104	45	108	73	105	63	111	81	-1.7	-3.5
CS3	A	1004	943	175	751	249	139	77	644	358	111	90	-29.2	-14.3
	B	1027	907	231	755	302	233	154	654	432	201	178	-23.9	-11.6
	C	1025	962	263	789	271	280	183	721	455	257	217	-32.3	-16.5
CS4	A	1060	1060	227	815	316	216	80	611	388	186	165	-27.6	-14.2
	B	966	955	220	-	-	-	-	-	-	-	-	-5.3	-1.2
	C	1013	968	241	782	295	224	136	649	387	186	142	-27.2	-14.5
CS5	A	982	967	249	760	271	215	135	626	370	203	165	-30.9	-15.8
	B	917	912	292	721	232	256	150	642	358	245	213	-10.9	-4.5
	C	1102	1040	290	810	355	271	209	673	392	222	190	-28.0	-13.7
CS6	A	933	907	211	851	264	186	139	634	381	178	159	-20.3	-9.5
	B	830	805	210	640	242	177	147	544	278	171	149	0.1	-1.5
	C	907	883	176	724	220	154	115	518	291	170	141	-22.7	-7.7
S1	A	1119	1110	312	903	246	300	179	747	480	309	289	-29.3	-15.6
	B	307	318	206	172	70	147	86	148	99	143	118	-2.3	-1.1
	C	105	49	105	50	37	88	65	35	34	68	60	-1.1	-1.4
S2	A	150	52	150	131	63	158	78	79	76	108	94	-1.3	-1.3
	B	1003	1003	312	729	138	300	121	872	709	301	270	-4.0 (18.0)	9.2
	C	163	66	163	48	39	98	69	48	44	100	86	-0.4 (1.1)	-0.4
S3	A	1146	1042	327	790	183	317	163	714	383	311	266	-18.8	-8.1
	B	433	431	298	390	118	267	160	258	145	245	192	-0.9 (5.5)	0.61
	C	1110	1089	341	815	245	316	177	851	437	313	263	-21.8	-11.0
S4	A	1147	1063	391	846	240	374	193	754	464	366	310	-18.0	-8.9
	B	1141	1042	414	863	243	373	175	752	461	363	281	-1.6	-1.2
	C	267	231	240	169	88	187	92	164	122	182	151	-1.8	-2.8
S5	A	1149	1031	387	781	261	380	189	774	494	355	312	-23.0	-13.9
	B	1137	1052	435	833	258	405	234	708	488	394	340	-3.0 (2.7)	-1.6
	C	1145	1064	401	813	214	348	170	771	365	362	290	-25.0	-14.4
B1	A	1198	998	491	876	192	444	241	666	310	462	336	-21.8	-13.0
	B	1112	1096	555	742	272	529	270	646	290	490	349	3.7 (-12.8)	-2.7
	C	1133	1015	491	877	238	483	264	672	312	403	314	-28.3	-18.8
B2	A	1188	958	300	1007	94	248	108	677	213	266	196	-	-
	B	1016	873	360	829	126	344	212	624	222	318	251	-	-
	C	1299	1104	340	996	173	316	188	706	285	289	223	-	-
B3	A	1150	1142	332	851	184	344	171	605	263	289	247	-29.6	-6.0
	B	1200	1200	401	1130	201	474	266	712	331	432	328	-4.3 (5.5)	4.1
	C	1249	1238	367	941	200	439	231	660	291	410	306	-31.6	-19.8
B4	A	1150	1141	295	671	142	211	118	529	312	216	249	-24.9	-10.2
	B	1127	1127	348	903	265	456	258	644	360	418	289	24.3	5.3
	C	1026	1026	326	890	196	359	183	627	303	334	243	-28.1	-18.5

-: the data were not measured.

Table 4 Fire resistance of six concrete slabs based on different failure criteria

Slab	Fire resistance (min)		
	Steel temperature failure criterion (A/B/C)	Concrete temperature failure criterion (A/B/C)	Deflection failure criterion (l/50) (A/B/C)
CS1	41.7/*/*	28.2/*/*	*/*/*
CS2	*/58.3/*	*/34.8/*	*/*/*
CS3	74.5/65.2/52.3	69.8/46.7/49.7	89.7/*/70.2
CS4	69.3/-/83.7	33.8/-/45.6	*/*/*
CS5	76.5/70.6/71.1	62.3/57.5/29.3	66.7/*/*
CS6	73.2/*/*	57.5/54.3/63.3	*/*/*
S1	123.5/*/*	100.0/*/*	*/*/*
S2	*/94.5/*	*/200.0/*	*/*/*
S3	81.0/*/40.0	122.5/193.5/95.5	*/*/*
S4	51.0/65.5/*	118.0/108.5/*	*/*/*
S5	41.5/86.5/52.5	103.5/116.0/128.5	*/*/*
B1	116.3/145.2/93.5	137.8/136.5/108.5	*/*/*
B2	79.8/127.5/103.2	190.5/169.1/110.3	-/-/-
B3	169.0/106.5/131.5	152.2/151.7/139.0	80.5/*/162.7
B4	*/123.8/133.0	178.0/102.2/140.5	*/*/*

Note: '*' no failure, '-' no data

Conflict of interest

The authors declared that they have no conflicts of interest to this work. We declare that we do not have any commercial or associative interest that represents a conflict of interest in connection with the work submitted.